2014 Spring

"Advanced Physical Metallurgy"
- Bulk Metallic Glasses -

04.15.2014

Eun Soo Park

Office: 33-313
Telephone: 880-7221
Email: espark@snu.ac.kr
Office hours: by appointment

Glass formation

Retention of liquid phase | **Formation of crystalline phases**

Alloy Design Optimization | **Process Optimization**

Consideration of Thermodynamic, Kinetic and Structural aspects for glass formation

Empirical Rules
Minor additions
Trial and Errors

1. Chemical etching of ingot
2. Vessel cleaning
3. Successive heating-cooling cycles in a molten oxide flux
4. Alloying at high temperature
5. Process with high cooling rate

Suppression of nucleation and growth of crystalline phase
➡ *High glass-forming ability(GFA)*

2.7.2 The Origins of BMGs

* History of Metallic Glasses

* First **amorphous metal** produced by evaporation in 1934.

  j. Kramer, Annalen der Phys. 1934; 19: 37.

* First **amorphous alloy**(CoP or NiP alloy)

  produced by electro-deposition in 1950.

  A. Brenner, D.E. Couch, E.K. Williams, J. Res. Nat. Bur. Stand. 1950: 44; 109.

* First **metallic glass** ($Au_{80}Si_{20}$)
  produced by splat quenching at Caltech by Pol Duwez in 1957.

  W. Klement, R.H. Willens, P. Duwez, Nature 1960; 187: 869.

* First **bulk metallic glass** ($Pd_{77.5}Cu_6Si_{16.5}$)
  produced by droplet quenching at Harvard Univ.
  by **H.S. Chen and D. Turnbull** in 1969

  H.S. Chen and D. Turnbull, Acta Metall. 1969; 17: 1021.

  produced by water quenching of PdTMSi, Pt-Ni-P and Pd-Ni-P system
  by **H.S. Chen** in 1974 (long glassy roads, 1-3 mm in diameter and several centimeters in length)

 *H.S. Chen, Acta Metall. 1974; 22: 1505*
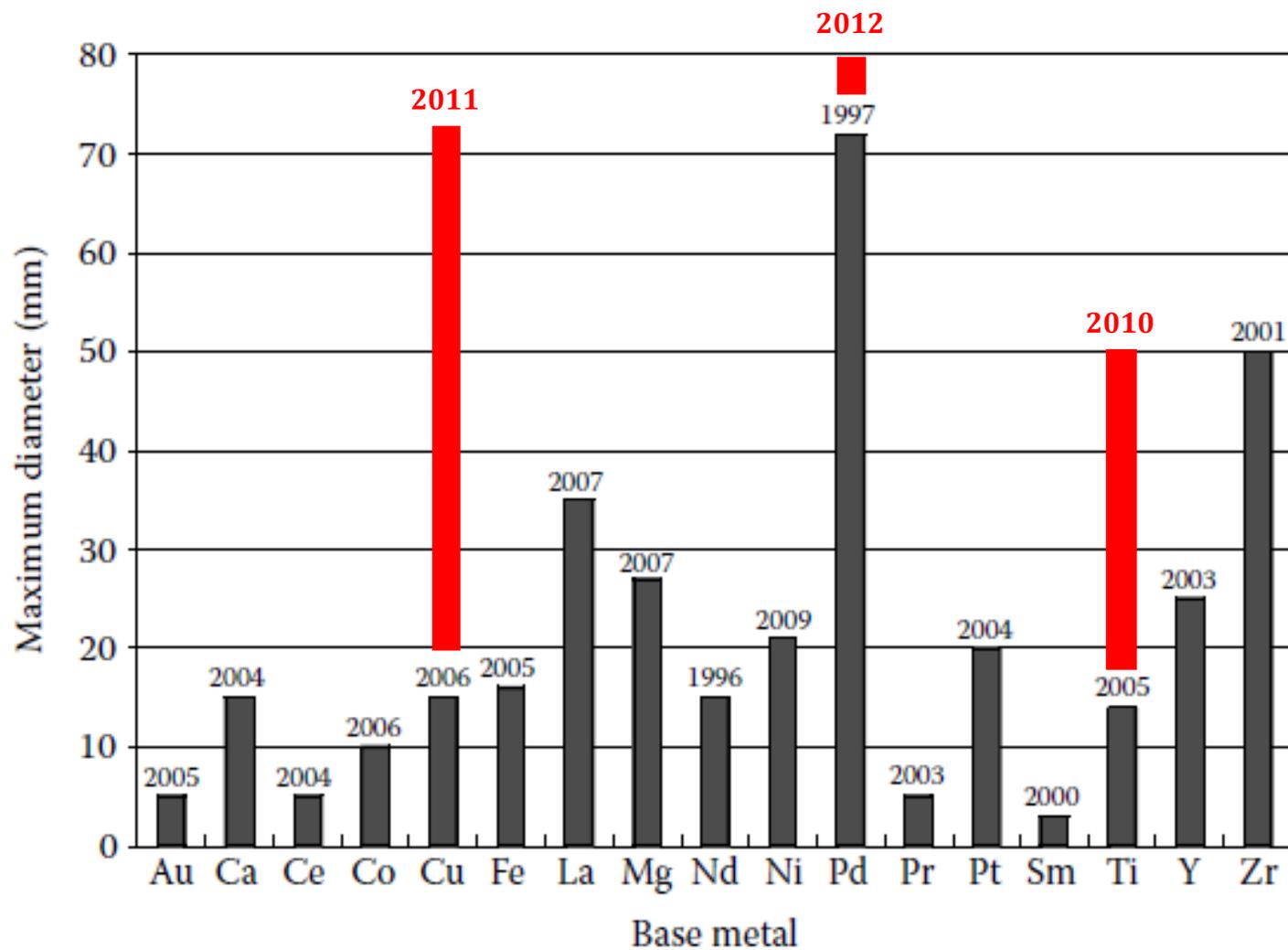
FIGURE 2.7
Maximum diameters of the BMG rods achieved in different alloy systems and the years in which they were discovered.

3. Glass-Forming Ability of Alloys

- **Many glasses were produced more or less by trial and error.**

   → **The ability of a metallic alloy to transform into the glassy state is defined in this chapter as the glass-forming ability (GFA).**

3.2 Critical Cooling Rate

   If an alloy melt is solidified from a temperature above the liquidus temperature, T_l to below the glass transition temperature, T_g, then the volume fraction of the solid crystalline phase, X formed under non-isothermal crystallization conditions can be given by the equation [8,9]

$$X(T) = \frac{4\pi}{3R^4} \int_{T_l}^{T_g} I(T') \left[\int_{T''}^{T_g} U(T'')dT'' \right]^3 dT' \tag{3.1}$$

where I and U are the steady-state nucleation frequency and crystal growth rate,

$\boxed{X = 10^{-6}}$ ➡

$$R_c^4 = \frac{4\pi}{3 \times 10^{-6}} \int_{T_l}^{T_g} I(T') \left[\int_{T''}^{T_g} U(T'')dT'' \right]^3 dT' \tag{3.2}$$

Since the equations for I and U contain terms like viscosity of the supercooled liquid, η, entropy of fusion, ΔS_f, etc., the critical cooling rate, R_c decreases with increasing η, ΔS_f, and decreasing liquidus temperature, T_l. The best way to experimentally determine R_c is by constructing the time–temperature–transformation (T–T–T) diagrams.

5

3.2.1 T-T-T Diagrams: isothermal processes

the liquid alloy should be cooled at a rate faster than R_c and to a temperature below T_g.

$$R_c \cong \frac{T_\ell - T_n}{t_n}$$
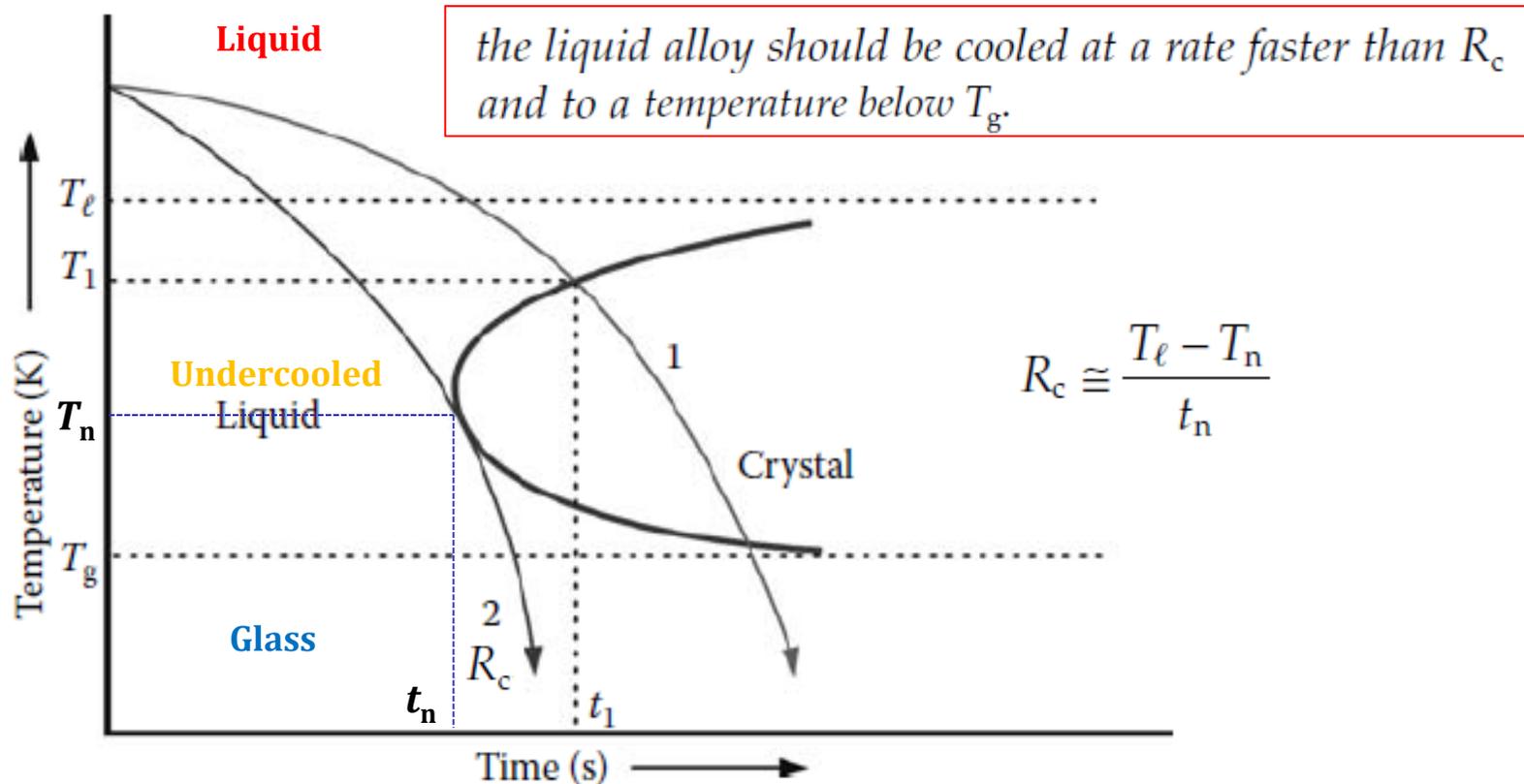
FIGURE 3.1

Schematic time–temperature–transformation (T–T–T) diagram for a hypothetical alloy system. When the liquid alloy is cooled from above the liquidus temperature T_ℓ, at a rate indicated by curve "1," solidification starts at a temperature T_1 and time t_1. The resultant product is a crystalline solid. However, if the same liquid alloy is now cooled, again from T_ℓ, at a rate faster than the rate indicated by curve "2," the liquid will continue to be in the undercooled state, and when cooled below the glass transition temperature T_g, the liquid is "frozen-in" and a glassy phase is formed. The cooling rate represented by curve "2" is referred to as the critical cooling rate, R_c.

# R_c vs D_{max} in Ti-Zr-Cu-Ni alloy system
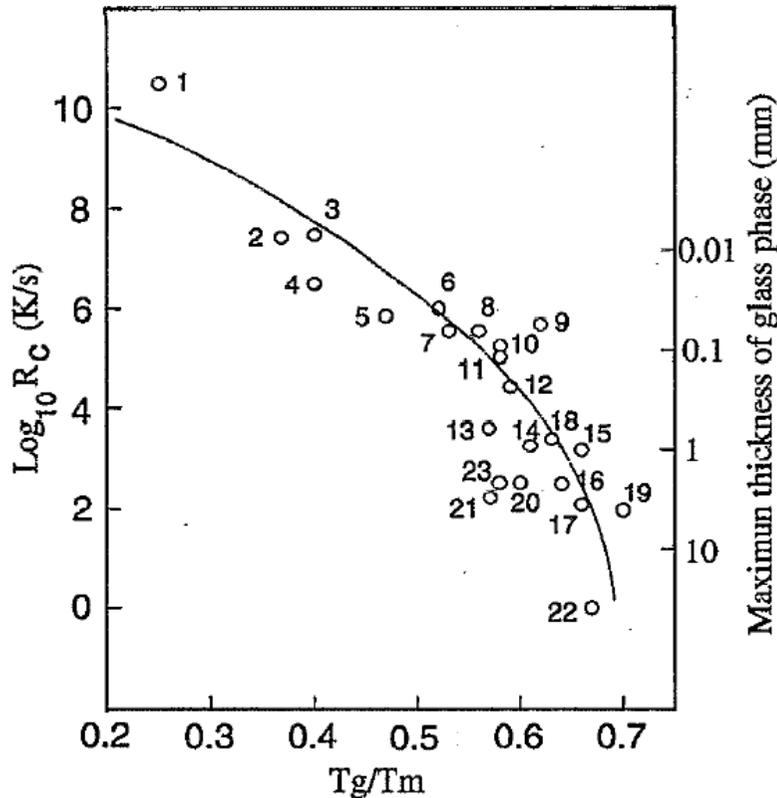
FIG. 1. Critical cooling rates for glass formation and corresponding maximum thickness of glass phase. Key to the alloys: (1) Ni; (2) $Fe_{91}B_9$; (3) $Fe_{89}B_{11}$; (4) Te; (5) $Au_{77.8}Ge_{13.8}Si_{8.4}$; (6) $Fe_{83}B_{17}$; (7) $Fe_{41.5}Ni_{41.5}B_{17}$; (8) $Co_{75}Si_{15}B_{10}$; (9) Ge; (10) $Fe_{79}Si_{10}B_{11}$; (11) $Ni_{75}Si_8B_{17}$; (12) $Fe_{80}P_{13}C_7$; (13) $Pt_{60}Ni_{15}P_{25}$; (14) $Pd_{82}Si_{18}$; (15) $Ni_{62.4}Nb_{37.6}$; (16) $Pd_{77.5}Cu_6Si_{16.5}$; (17) $Pd_{40}Ni_{40}P_{20}$ (above from Ref. 3); (18) $Au_{55}Pb_{22.5}Sb_{22.5}$ (Ref. 6); (19) $La_{55}Al_{25}Ni_{10}Cu_{10}$ (Ref. 7); (20) $Mg_{65}Cu_{25}Y_{10}$ (Ref. 8); (21) $Zr_{65}Cu_{17.5}Ni_{10}Al_{7.5}$ (Ref. 9); (22) $Zr_{41.2}Ti_{13.8}Cu_{12.5}Ni_{10}Be_{22.5}$ (Refs. 4 and 5); (23) $Ti_{34}Zr_{11}Cu_{47}Ni_8$.

Total cooling time $\tau \sim (R^2/\kappa)$

sample dimension (dia. or thickness) : R
initial temperature: T_m
thermal diffusivity : κ

$\kappa = K/C$

thermal conductivity : K
heat capacity per unit volume: C

$$\dot{T} = \frac{dT}{dt} = \frac{(T_m - T_g)}{\tau} = \frac{K(T_m - T_g)}{CR^2}$$

For Ti-Zr-Cu-Ni system,

$T_m - T_g \sim 400K$ $K \sim 0.1 W/cm\ s^{-1}K^{-1}$ $C \sim 4J/cm^3K^{-1}$

$$\dot{T}(K/s) = 10/R^2 (cm)$$

3.2.2. Effect of Alloying Elements
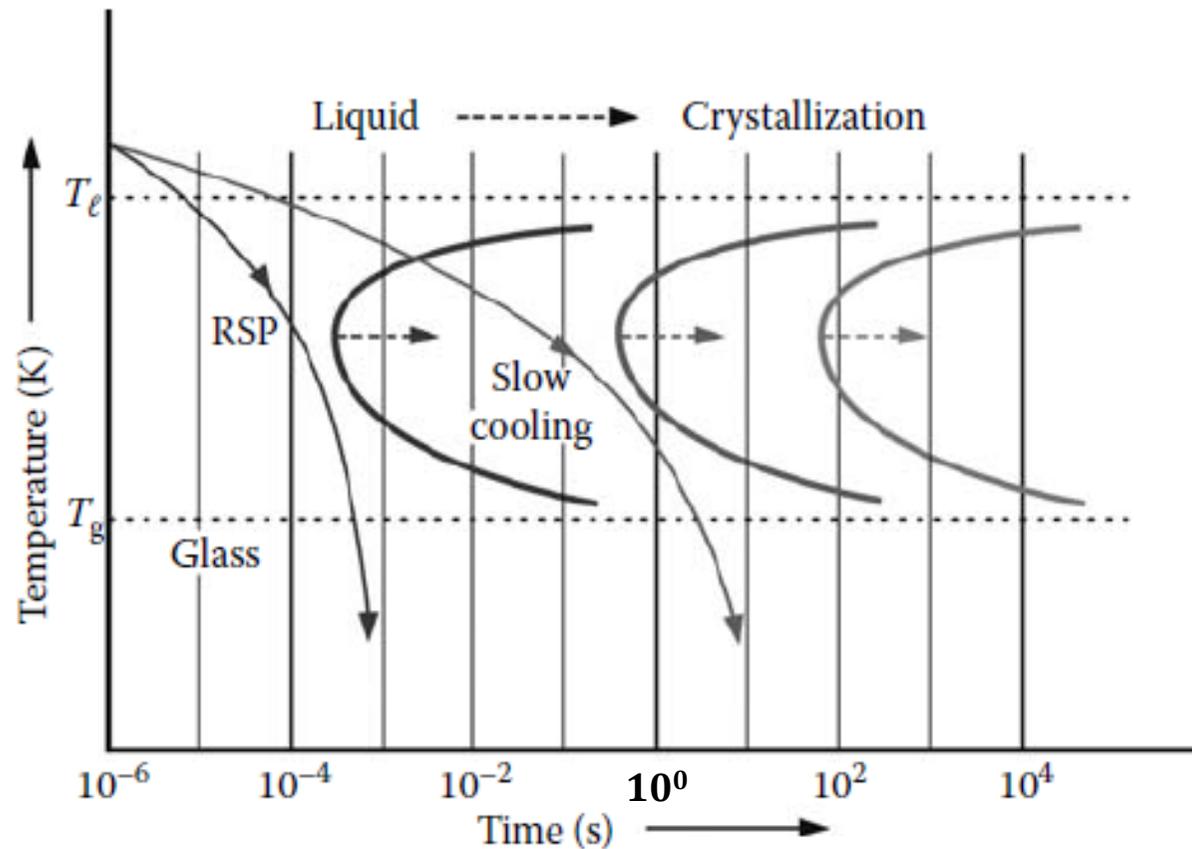
FIGURE 3.2

Position of the T–T–T curves with the addition of a large number of alloying elements. The C-curve shifts to the right with increasing number of alloying elements and consequently, the glassy phase can be synthesized at slow solidification rates. The left-most C-curve represents a typical situation of an alloy system where a glassy phase is obtained by rapid solidification processing (RSP) from the liquid state. The middle C-curve represents an alloy composition where a glassy phase can be obtained by slow cooling. The right-most C-curve represents a situation when an alloy can be very easily produced in a glassy state.

R_c

> 10^{10-12} K/s 10^{4-6} K/s 10^2 K/s 1.3×10^{-2} or 0.067 K/s 10^{-5} to 10^{-4} K/s

pure metals   binary   typically $Pd_{37.5}Cu_{32.5}Ni_{10}P_{20}$ Oxide glasses
metallic liquids multicomponent $Pd_{30}Pt_{17.5}Cu_{32.5}P_{20}$

$$R_c = \frac{\Delta T}{t_n}$$

PdCuSi $R_c = 3.5 \times 10^1$ K/s

PdSi $R_c = 3 \times 10^3$ K/s

AuGeSi $R_c = 10^6$ K/s

Ni $R_c = 10^{10}$ K/s

FIGURE 2.3
Time–temperature–transformation (T–T–T) curves (solid lines) and the corresponding contin-
uous cooling transformation curves (dashed lines) for the formation of a small volume fraction
for pure metal Ni, and $Au_{78}Ge_{14}Si_8$, $Pd_{82}Si_{18}$, and $Pd_{78}Cu_6Si_{16}$ alloys.

T_{rg} 1/4   1/2   2/3

(a) Measurement of TTT diagram during cooling by DSC/DTA

Measuring upper part of TTT diagram

Temperature (K)

T_l

hard to pass the nose point

S.C. liquid

Bottle neck

crystal

T_g

Time(s)

T_{liq}

T_g

$Pd_{40}Cu_{30}Ni_{10}P_{20}$

temperature (K)

time (s)

$T_{empty\ crucible} - T_{sample}$

50 s

time (s)

temperature (K)

$Pd_{40}Cu_{30}Ni_{10}P_{20}$

time (s)
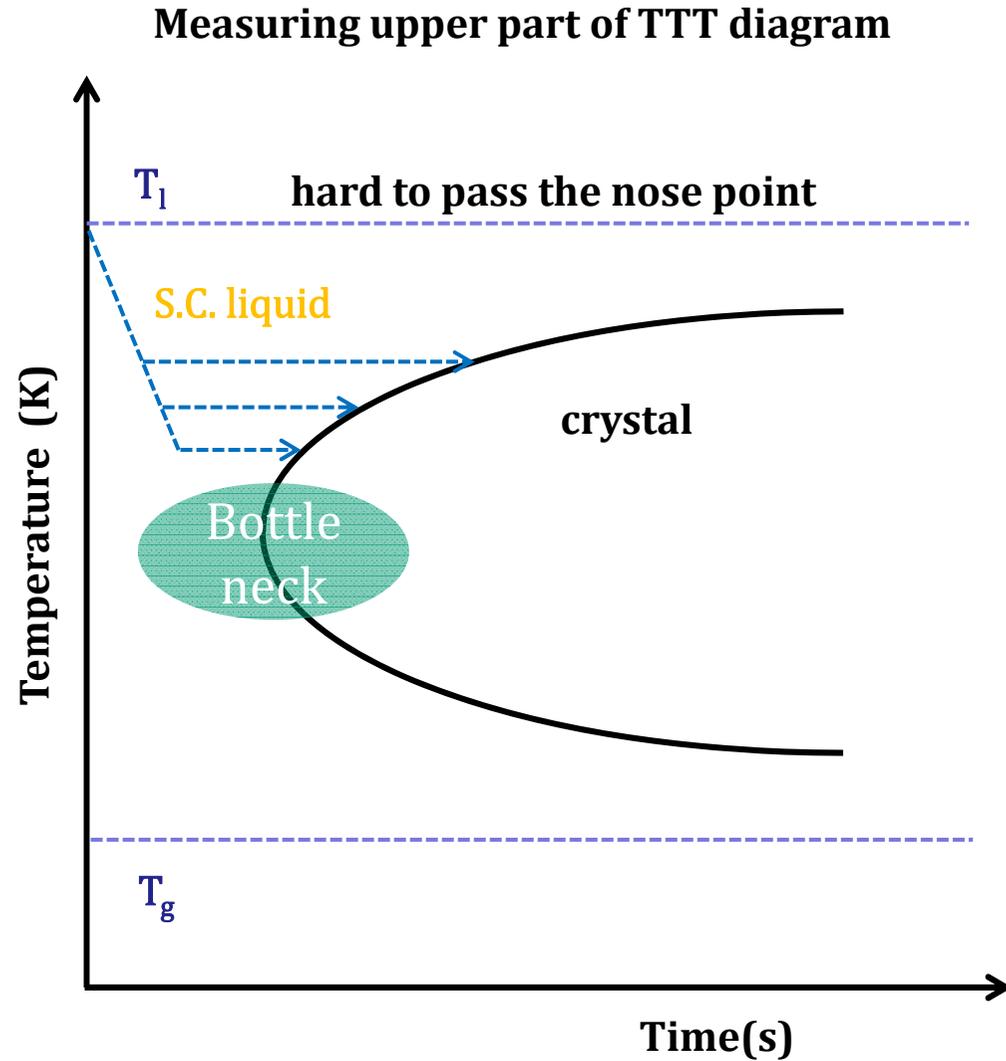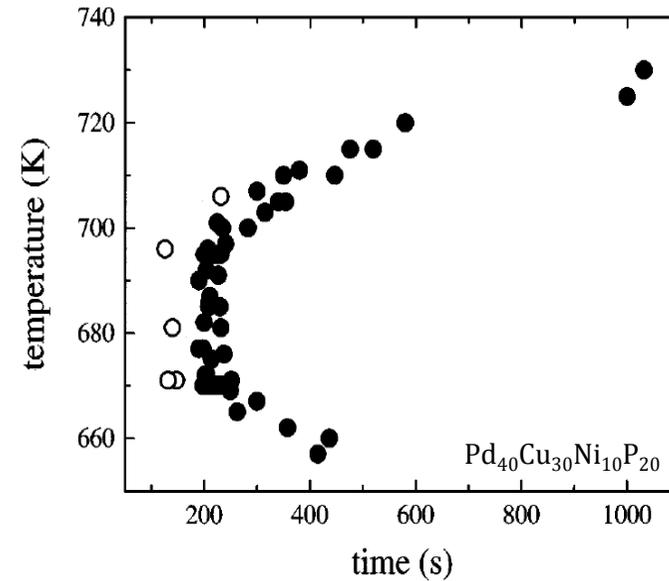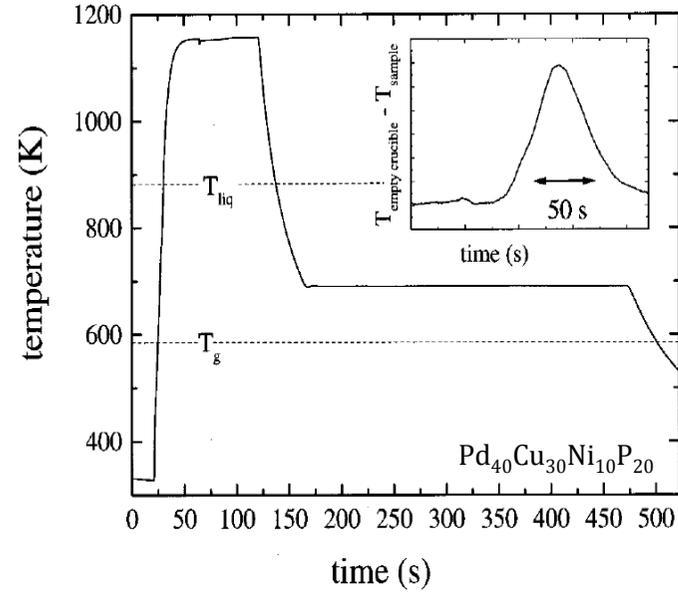
TTT diagram of $Pd_{40}Cu_{30}Ni_{10}P_{20}$

$T_{liq} = 823$ K

$T_g = 582$ K

2.8K/s

0.11K/s

0.33K/s
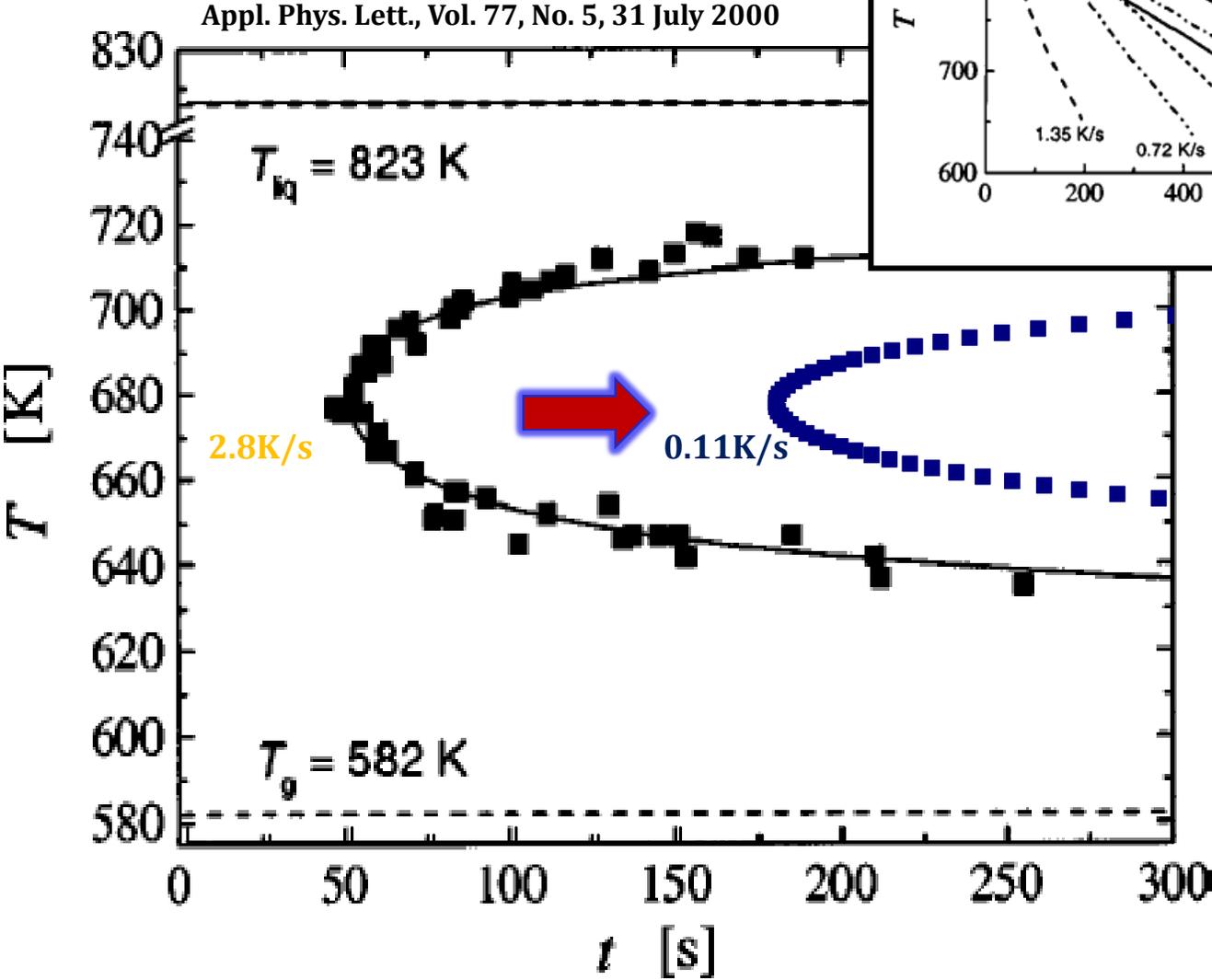
# (b) Measurement of TTT diagram by drop tube technique

Solidification of containerless undercooled Melts, edited by Dieter M. Herlach and Douglas M. Matson, 2012, p.1-7
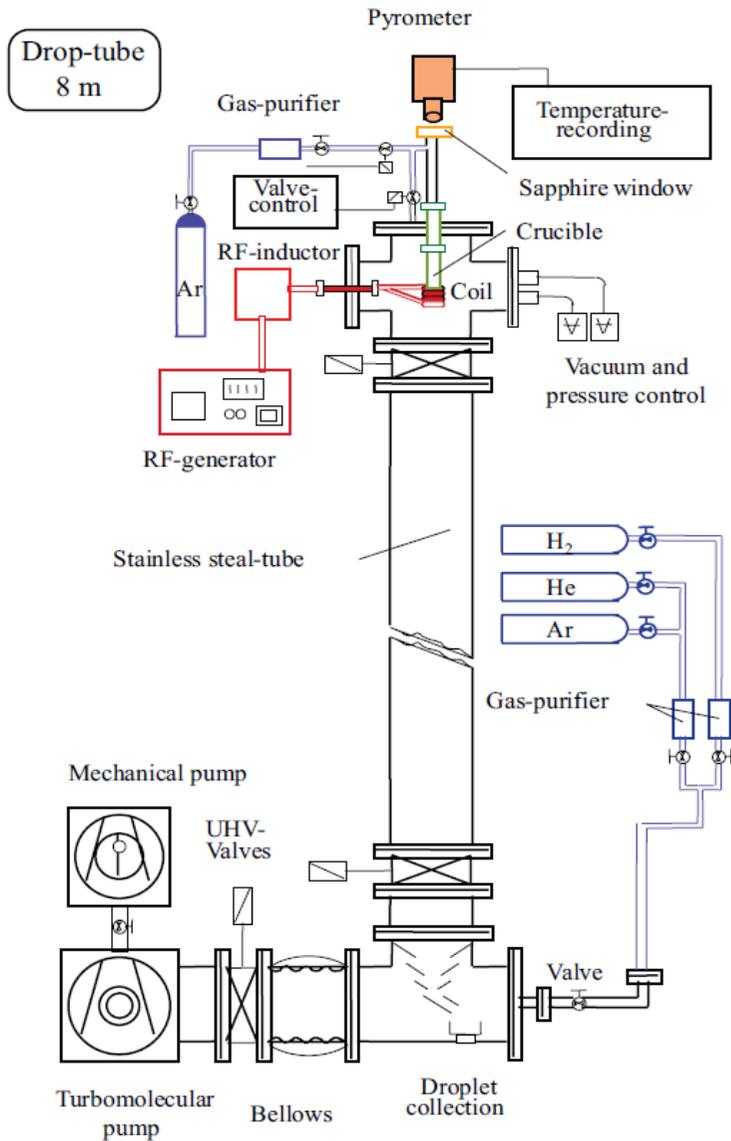

Schematic view of DLR drop tube

Drop tube technique

- **rapid cooling of small particles**
  by dispersion of the melt

- **reduction of heterogeneous nucleation**
  by containerless processing
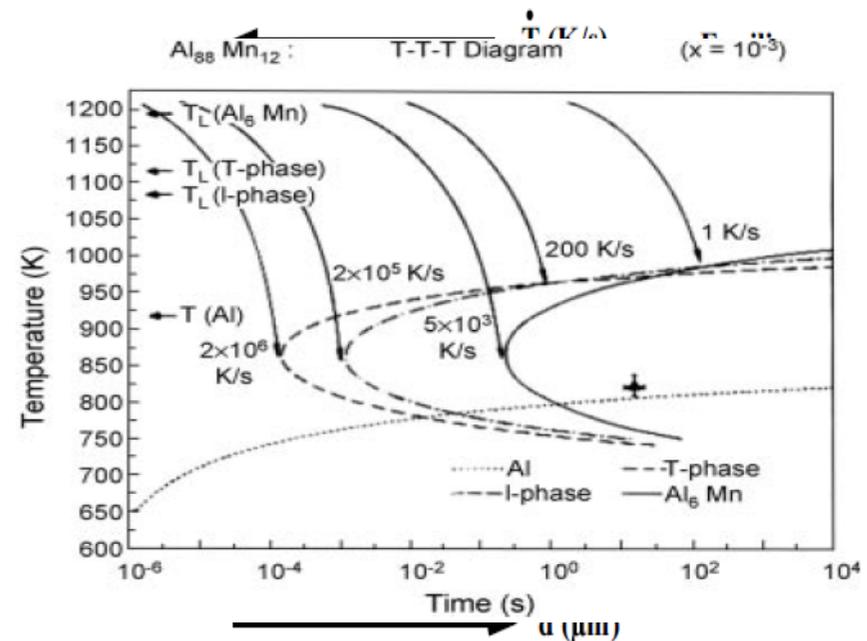
- TTT diagram of the solidification of phases involved in the solidification of undercooled droplets of $Al_{88}Mn_{12}$

12

Electrostatic levitation in KRISS

HV (z-axis)

T : ~3000 °C
P : ~ 10^{-7} Torr

Heating laser

He-Ne laser

He-Ne laser

Feedback

PSD (x)

PSD (y)

HV (x-axis)

**HV (y-axis)**

Feedback

KRISS material : Dr. G.W.Lee
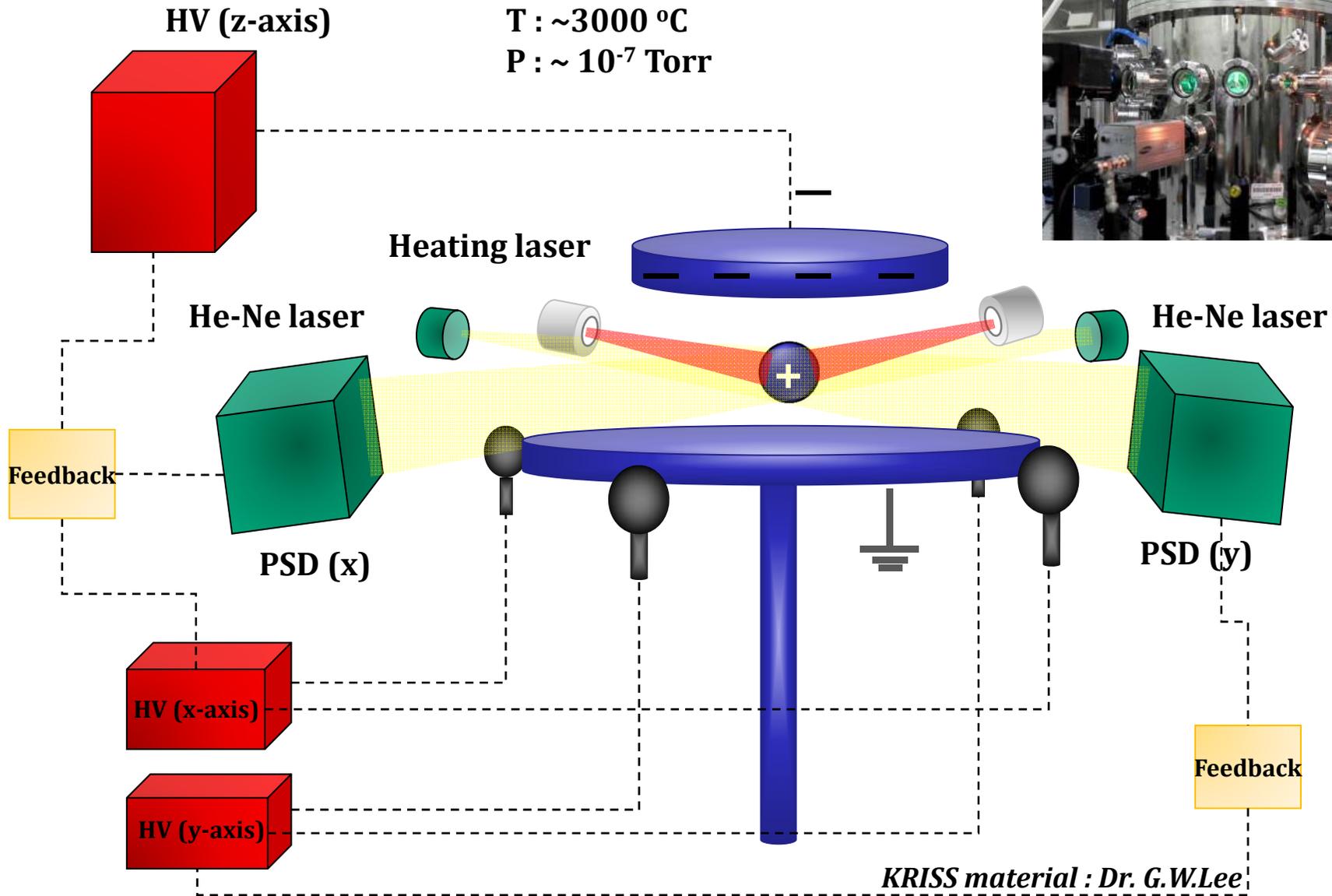
Measurement of TTT diagram by ESL technique

* Isothermal annealing in containerless condition
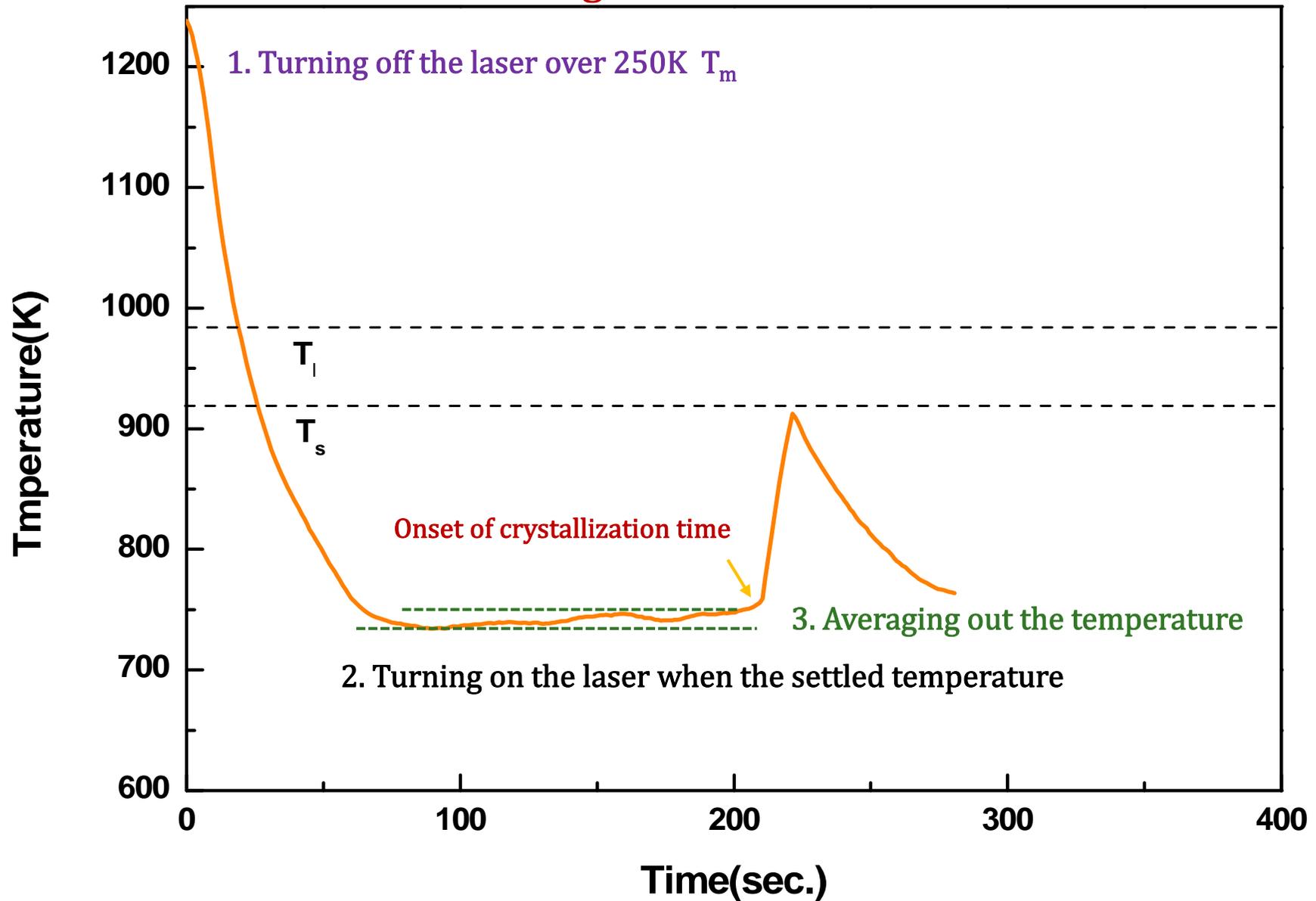
Comparison of TTT diagrams: TZ3 vs ZCAAB vs VIT1 vs PNCP
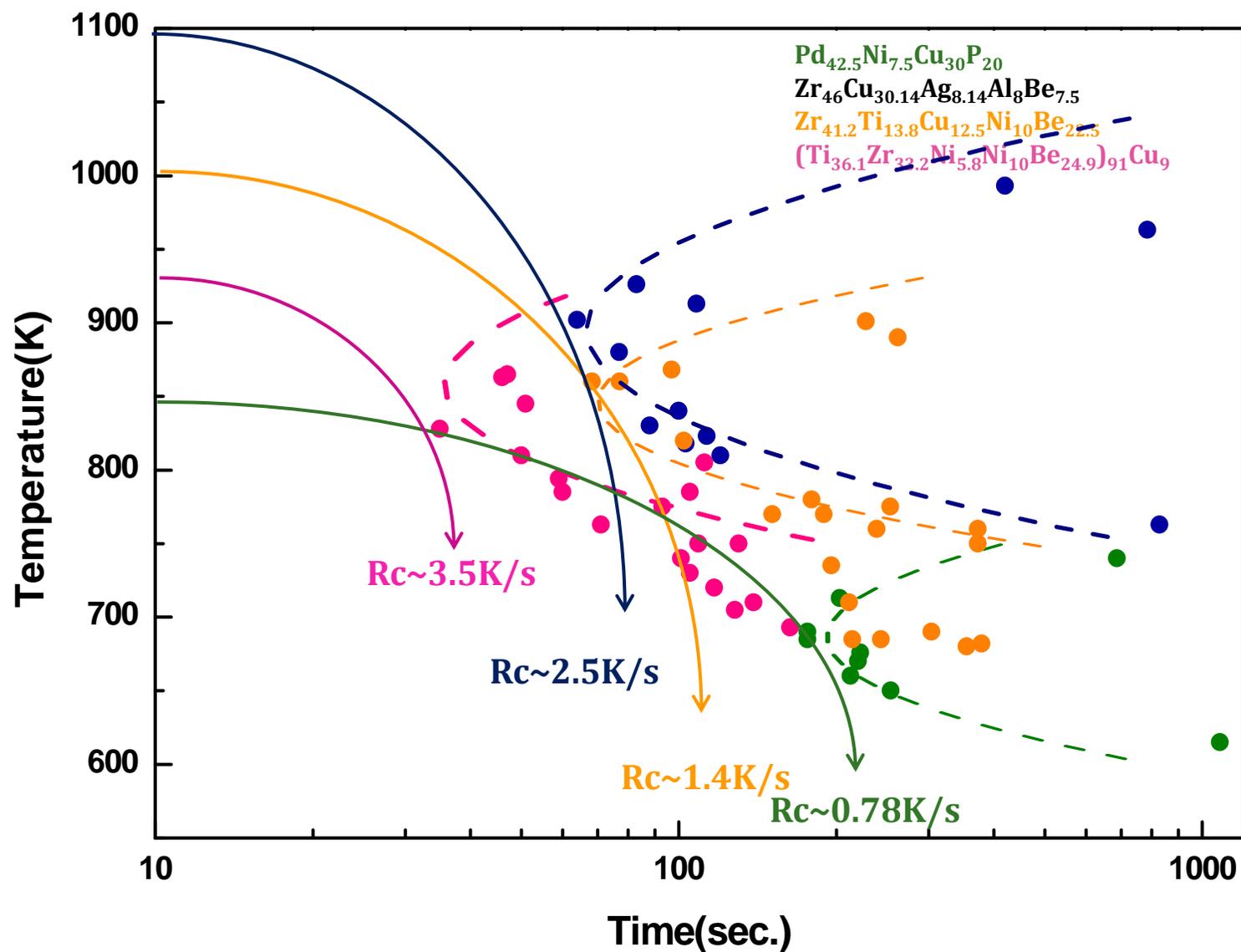
Comparison of TTT diagrams: TZ3 vs ZCAAB vs VIT1 vs PNCP
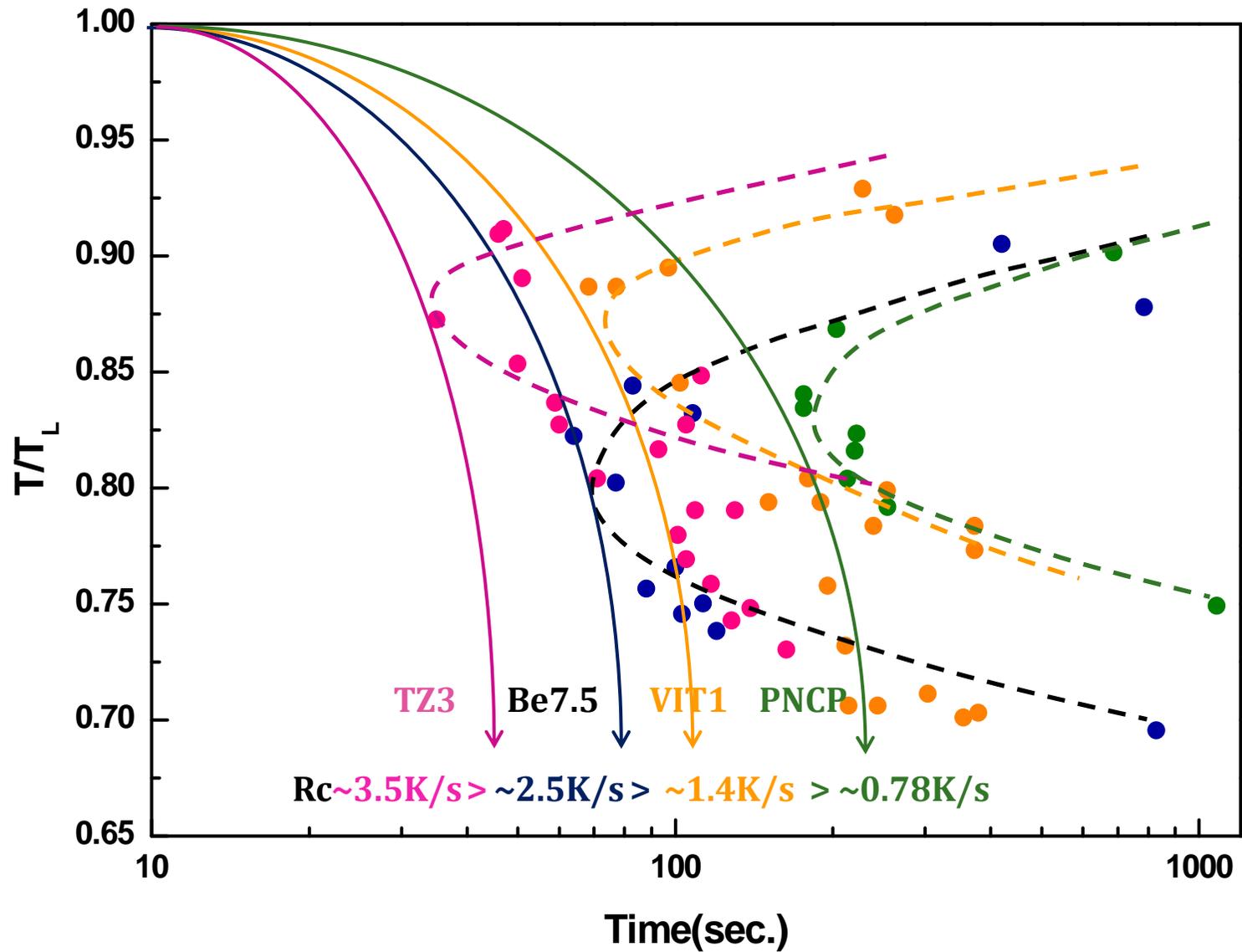
3.2.3 Measurement of R_c

The measurement of R_c is an involved and time-consuming process. One has to take a liquid alloy of a chosen composition and allow it to solidify at different cooling rates and determine the nature and amount of phases formed after solidification.

Measurement of R_c in $Ca_{65}Mg_{15}Zn_{20}$ ($D_{max} > 15$ mm)

$$R_c = \frac{T_i - T_g}{\Delta t}$$

$Ca_{65}Mg_{15}Zn_{20}$
(Cu mold casting in air atmosphere)

(c) d = 15 mm

T_l

(b) d = 10 mm

45 mm

(a) d = 6 mm

T_g

(a) (b) (c)

top position : 20 K/s

middle position : 93 K/s

bottom position : 149 K/s
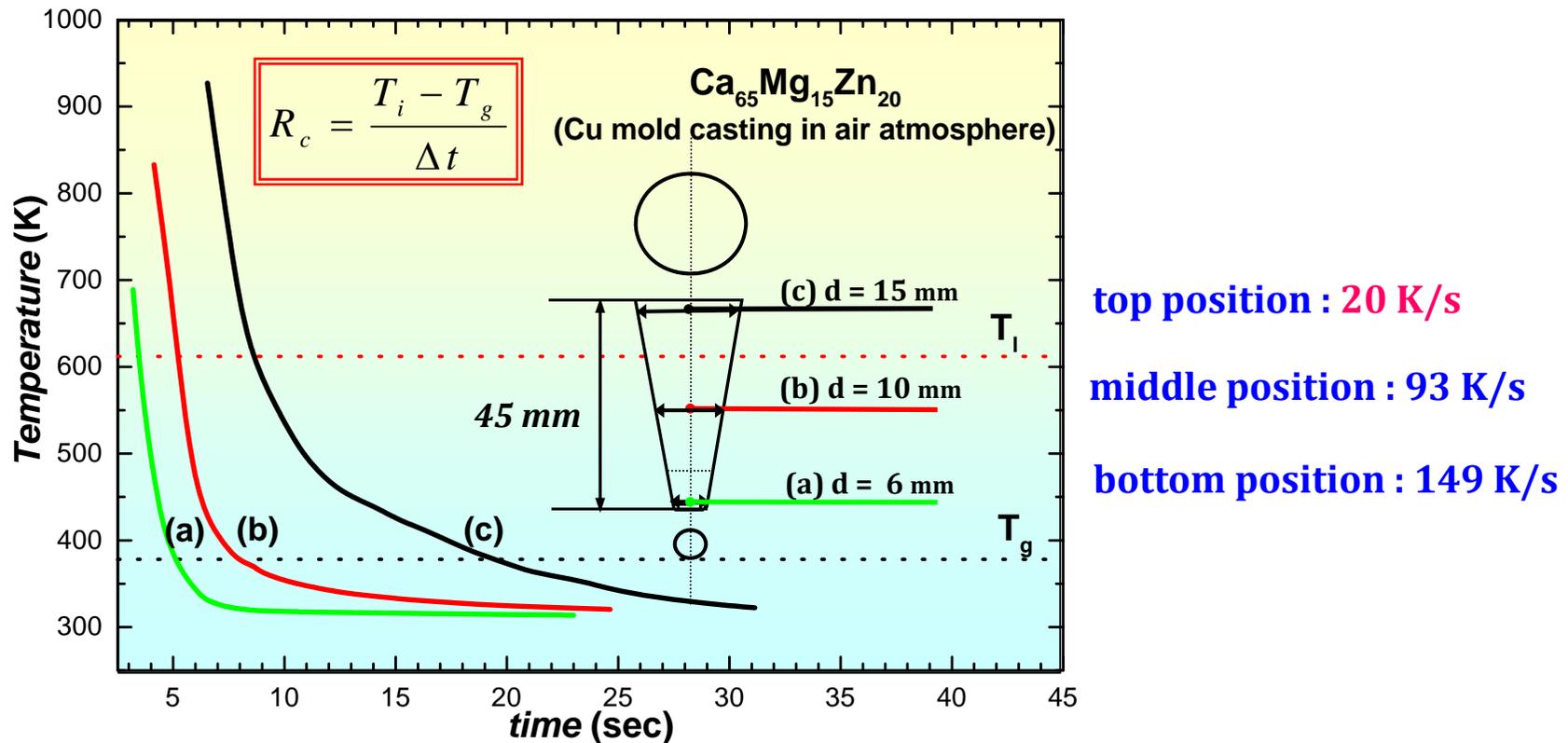
* Cooling curves measured at the center of the three transverse cross sections

* J. Mater. Res. 19, 685 (2004)
* Mater. Sci. Forum 475-479, 3415 (2005)

Measurement of R_c in Mg BMG (D_{max}=14 mm)
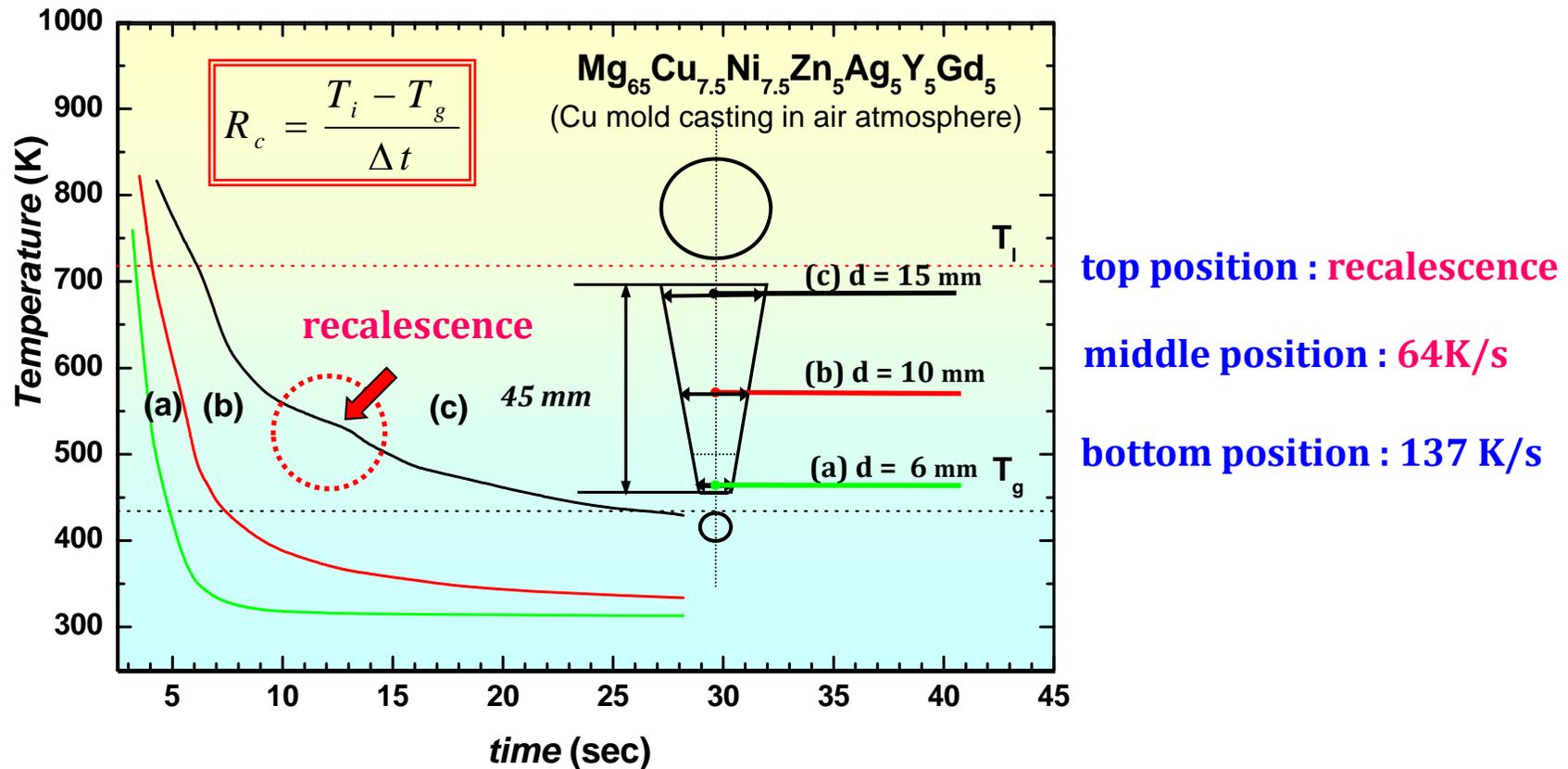
$$R_c = \frac{T_i - T_g}{\Delta t}$$

$Mg_{65}Cu_{7.5}Ni_{7.5}Zn_5Ag_5Y_5Gd_5$
(Cu mold casting in air atmosphere)

recalescence

(a) (b) (c)   45 mm

(c) d = 15 mm

(b) d = 10 mm

(a) d = 6 mm T_g

T_l

Temperature (K) — 1000, 900, 800, 700, 600, 500, 400, 300

time (sec) — 5, 10, 15, 20, 25, 30, 35, 40, 45

top position : recalescence

middle position : 64K/s

bottom position : 137 K/s

* **Cooling curves** measured at the center of the three transverse cross sections

TABLE 3.1

Some Representative Critical Cooling Rates (R_c) for Formation of Glassy Phases in Different Alloy Systems

1) Effect of B_2O_3 fluxing

$Pd_{40}Cu_{30}Ni_{10}P_{20}$ $1.58\,K\,s^{-1}$ without fluxing [22]

$0.1\,K\,s^{-1}$ with fluxing [18]

2) Effect of # of components

$Pd_{82}Si_{18}$ $1.8 \times 10^3\,K\,s^{-1}$ $\longleftrightarrow$ $550\,K\,s^{-1}$ $Pd_{78}Cu_6Si_{16}$

$Cu_{50}Zr_{50}$ $250\,K\,s^{-1}$ $\longleftrightarrow$ $\leq 40\,K\,s^{-1}$ $Cu_{48}Zr_{48}Al_4$

3) Nature of alloying addition

$Mg_{65}Cu_{25}Y_{10}$ $Mg_{65}Cu_{25}Gd_{10}$ $Mg_{65}Cu_{15}Ag_5Pd_5Gd_{10}$

$100\,K\,s^{-1}$ $\longleftrightarrow$ $1\,K\,s^{-1}$ $\longleftrightarrow$ $0.7\,K\,s^{-1}$

Alloy Composition	R_c (K s^{-1})	Reference
$Au_{77.8}Ge_{13.8}Si_{8.4}$	3×10^6	[24]
$Ca_{60}Mg_{25}Ni_{15}$	24	[25]
$Ca_{65}Mg_{15}Zn_{20}$	<20	[26]
$Cu_{50}Zr_{50}$	250	[27]
$Cu_{48}Zr_{48}Al_4$	<40	[27]
$Cu_{42}Zr_{42}Ag_8Al_8$	4.4	[28]
$Fe_{43}Cr_{16}Mo_{16}C_{10}B_5P_{10}$	100	[29]
$Fe_{40}Ni_{40}P_{14}B_6$ (Metglas 2826)	4.4×10^7	[30]
$Hf_{70}Pd_{20}Ni_{10}$	124	[31]
$La_{55}Al_{25}Cu_{20}$	58	[32]
$La_{55}Al_{25}Ni_{20}$	69	[32]
$Mg_{65}Cu_{25}Gd_{10}$	1	[16]
$Mg_{65}Cu_{25}Y_{10}$	100	[33]
$Mg_{65}Cu_{15}Ag_5Pd_5Gd_{10}$	0.7	[34]
$Mg_{65}Cu_{7.5}Ni_{7.5}Ag_5Zn_5Gd_5Y_5$	20	[35]
$Nd_{60}Co_{30}Al_{10}$	4	[36]
$Ni_{62}Nb_{38}$	57	[37]
$Ni_{65}Pd_{15}P_{20}$	10^5	[38]
$Pd_{78}Cu_6Si_{16}$	550	[39]
$Pd_{40}Ni_{40}P_{20}$	128	[22]
$Pd_{42.5}Cu_{30}Ni_{7.5}P_{20}$	0.067	[18]
$Pd_{40}Cu_{25}Ni_{15}P_{20}$	0.150	[18]
$Pd_{40}Cu_{30}Ni_{10}P_{20}$ (without fluxing)	1.58	[22]
$Pd_{40}Cu_{30}Ni_{10}P_{20}$ (with flux treatment)	0.1	[18]
$Pd_{30}Pt_{17.5}Cu_{32.5}P_{20}$	0.067	[19]
$Pd_{82}Si_{18}$	1.8×10^3	[40]
$Pd_{82}Si_{18}$	800	[41]
$Pd_{81}Si_{19}$ (with flux treatment)	6	[42]
$Zr_{65}Al_{7.5}Ni_{10}Cu_{17.5}$	1.5	[43]
$Zr_{41.2}Ti_{13.8}Cu_{12.5}Ni_{10.0}Be_{22.5}$	1.4	[44]
$Zr_{46.25}Ti_{8.25}Cu_{7.5}Ni_{10.0}Be_{27.5}$	28	[44]
$Zr_{57}Cu_{15.4}Ni_{12.6}Al_{10}Nb_5$	10	[45]

Glass formation

Retention of liquid phase

Formation of crystalline phases

Thermodynamical point
Small change in free E. (liq.→ cryst.)

Kinetic point
Low nucleation and growth rates

Structural point
Highly packed random structure

Empirical rules
(1) multi-component alloy system   (2) significant difference in atomic size ratios
(3) negative heats of mixing   (4) close to a eutectic composition
(5) compositions far from a Laves phase region

- **Higher** degree of dense random packed structure

- **Suppression** of nucleation and growth of crystalline phase

➡ **High glass-forming ability (GFA)**

3.3 Reduced Class Transition Temperature (Kinetic aspect for glass formation)

T_{rg} **parameter** $= T_g/T_l \sim \eta$ **: the higher** T_{rg}**, the higher** η**, the lower** R_c

: ability to avoid crystallization during cooling
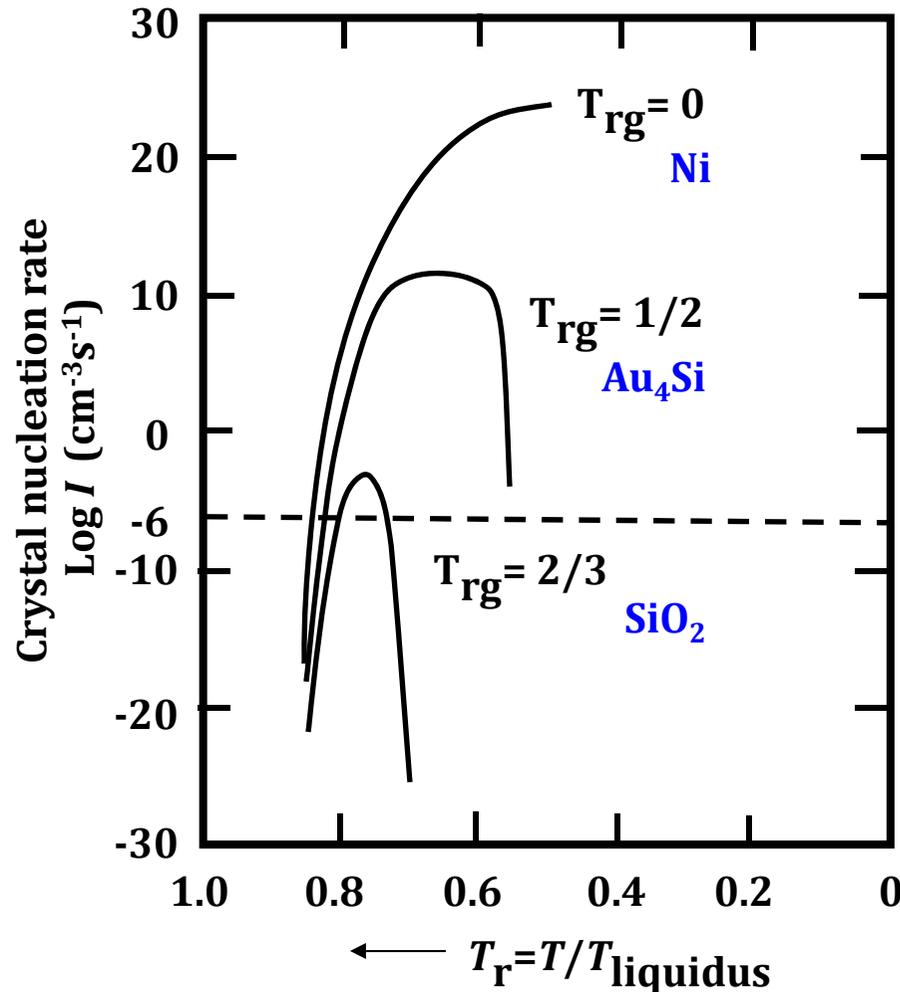
$T_{rgNi} < T_{rgAu4Si} < T_{rgSiO2}$

$R_{Ni} > R_{Au4Si} > R_{SiO2}$

Turnbull, 1959 ff.

- Based on the nucleation theory, Turnbull suggested that at $T_{rg} \geq 2/3$, homogeneous nucleation of the crystalline phase is completely suppressed. Most typically, a minimum value of $T_{rg} \sim 0.4$ has been found to be necessary for the glass to form.

- One should note the T_l, liquidus temperature as the point at the end of the liquid formation, and not at the beginning of melting.

TABLE 3.2

Reduced Glass Transition Temperatures (T_{rg}) for Different Glass-Forming Alloys

Alloy Composition	T_{rg}	References
$Ca_{65}Al_{35}$	0.69	[47]
$Ca_{67}Mg_{19}Cu_{14}$	0.60	[48]
$Ca_{57}Mg_{19}Cu_{24}$	0.64	[48]
$Cu_{65}Hf_{35}$	0.62	[49]
$Cu_{49}Hf_{42}Al_9$	0.62	[50]
$Cu_{64}Zr_{36}$	0.64	[51]
$La_{55}Al_{25}Ni_{20}$	0.71	[32]
$La_{62}Al_{15.5}(Cu,Ni)_{22.3}$	0.58	[52]
$La_{50.2}Al_{20.5}(Cu,Ni)_{29.3}$	0.47	[52]
$Ni_{62}Nb_{38}$	0.60	[37]
$Ni_{61}Nb_{33}Zr_6$	0.49	[53]
$Pd_{40}Ni_{40}P_{20}$	0.67	[54]
$Pd_{40}Cu_{30}Ni_{10}P_{20}$	0.67	[18,55]
$Zr_{41.2}Ti_{13.8}Cu_{12.5}Ni_{10}Be_{22.5}$	0.624	[45]
$Zr_{45.38}Ti_{9.62}Cu_{8.75}Ni_{10}Be_{26.25}$	0.50	[44]

- The concept of T_{rg} was introduced for kinetic reasons with the need to avoid crystallization [46]. It is known (and we will discuss this in some detail in Section 3.4) that T_g is a very weak function of the solute content, i.e., T_g varies much more slowly with solute concentration than the liquidus temperature, T_l. Consequently, the value of T_{rg} increases with increasing solute content, up to the eutectic composition, and therefore it becomes easier to avoid crystallization of the melt at the eutectic composition [13]. This reasoning seems to work well in simple binary alloy systems. But, in the case of multicomponent alloy systems such as the BMG compositions, the values of T_g and T_l vary significantly. Since the variation of viscosity with temperature is different for different alloy systems (and depends on whether a glass is strong or fragile), T_g alone may not provide information about the variation of viscosity with temperature and therefore, the T_{rg} criterion may not be valid in some systems.

Easy glass formation at compositions corresponding to high T_{rg} can be easily realized in alloy systems that feature deep eutectic reactions in their phase diagrams, and this is further explained in Section 3.4.

3.4 Deep Eutectics (Thermodynamic aspect for glass formation)

● **High GFA : low free energy** $\boxed{\Delta G(T)}$

   for transformation of liquid to crystalline phase

$$\boxed{\Delta G(T) = \Delta H_f - T\Delta S_f} \qquad \Delta G \Downarrow \;\rightarrow\; \Delta H_f \Downarrow \;\&\; \Delta S_f \Uparrow$$

Enthalpy of fusion   Entropy of fusion

$\Delta S_f \Uparrow$ **: proportional to the number of microscopic states**

Entropy of fusion   **Multi-component alloy systems** containing more than 3 elements

   causes an increase in the degree of dense random packing

$\Delta H_f \Downarrow$ **Large negative enthalpy of mixing** among constituent elements

Enthalpy of fusion

* **The free energy at a constant temperature also decreases in the cases of low**
chemical potential caused by low enthalpy and high reduced glass transition
temperature (=T_l/T_g) and high interface energy between liquid and solid phase.

3.4 Deep Eutectics (Thermodynamic aspect for glass formation)

ΔH_f ⬇ → **deep eutectic condition**: **increase stability of stable liquid (= T_g/T_l ↑)**

- decreasing melting point → less supercooled at T_g → $\Delta G = G^{liq} - G^{cryst}$ ⬇

ex) metallic / inorganic system
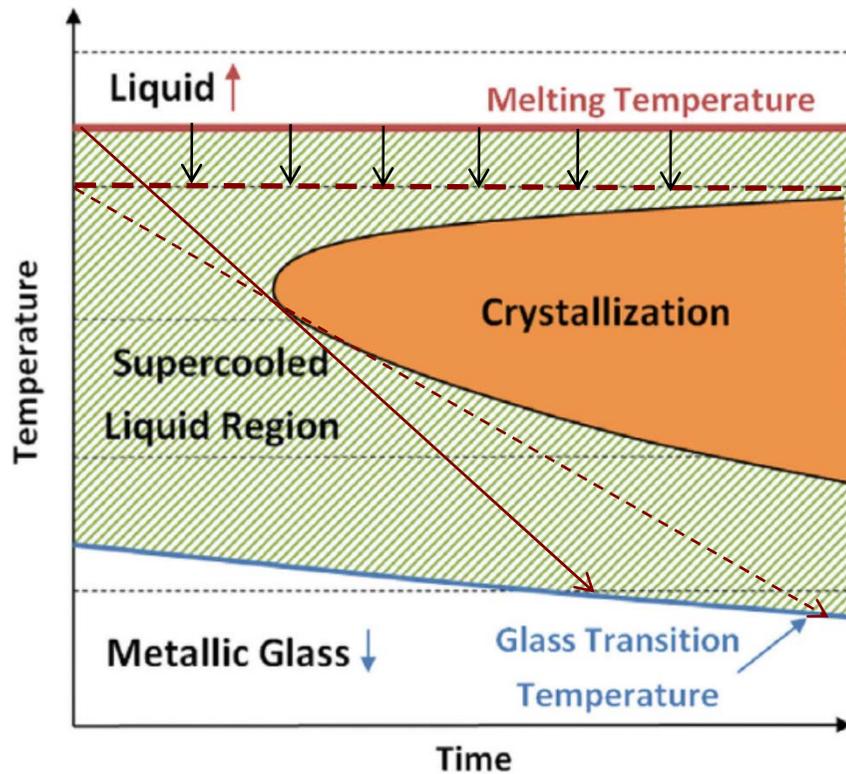
Glass forming region:
Compositions near the eutectic
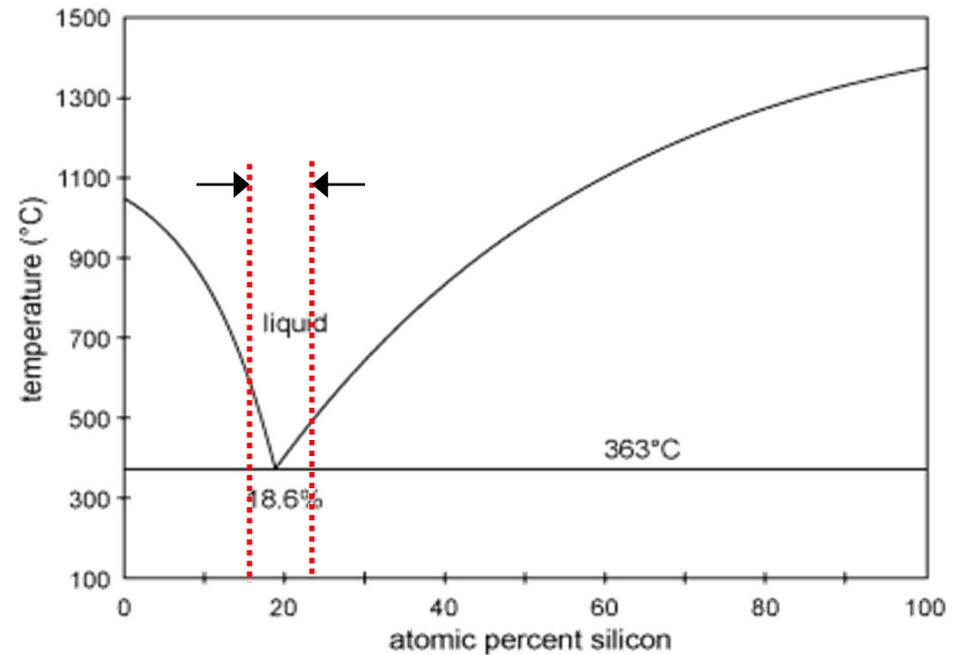
# Multi-component eutectic alloys with strong negative heat of mixing

less supercooled at T_g → $\Delta G = G^{liq} - G^{cryst}$

T_g : also changes depending on alloy composition

P. Haasen, Physical Metallurgy 3rd ed

Deep eutectic

L

α β

$\alpha + \beta$

T_ℓ

T_g

T_{rg}

$T_{rg}\sim$ highest value at eutectic composition

Shallow eutectic

L

α β

$\alpha + \beta$

T_ℓ

T_g

T_{rg}

$T_{rg}\sim$ may not be high at eutectic composition

A   Composition   B
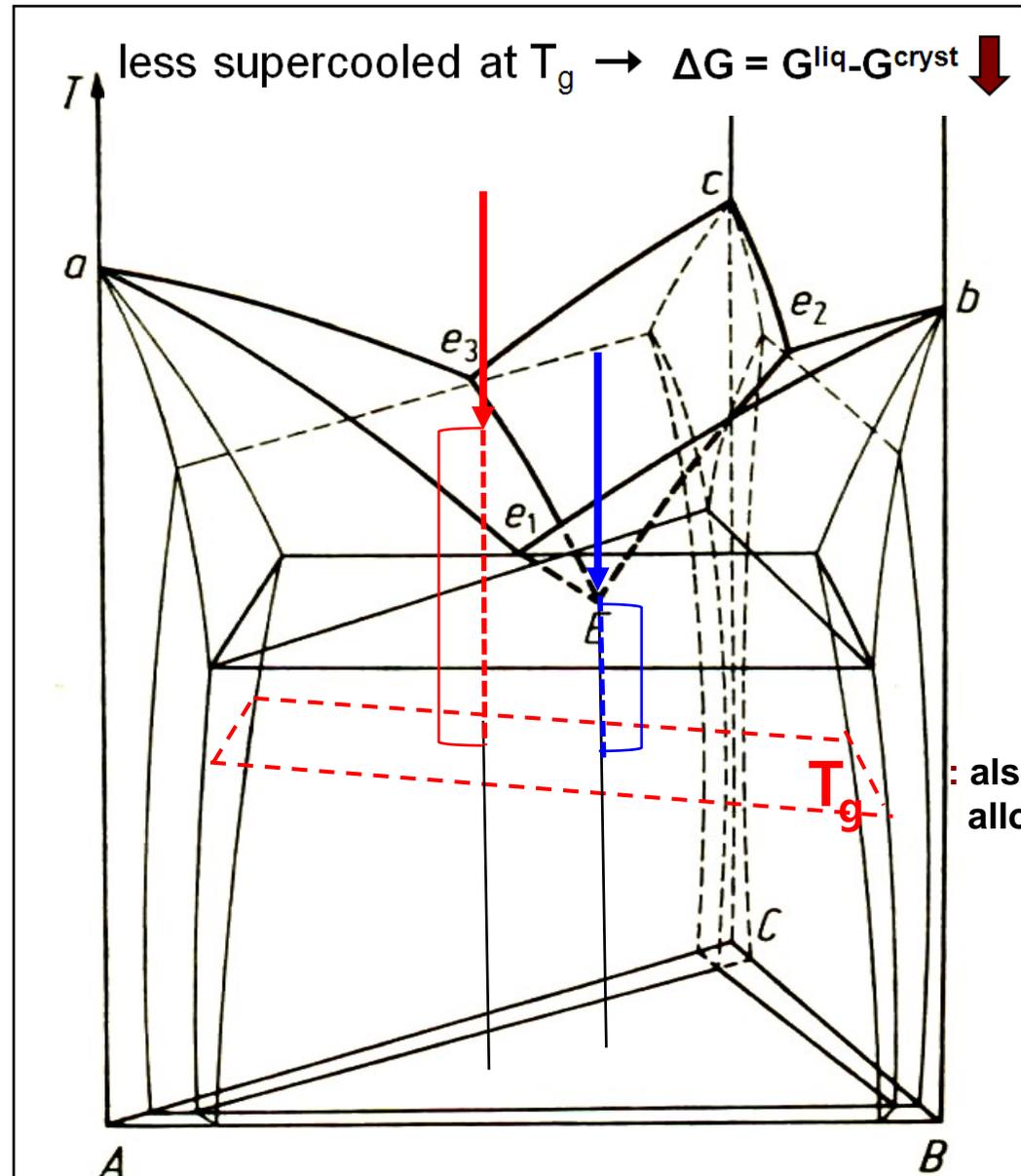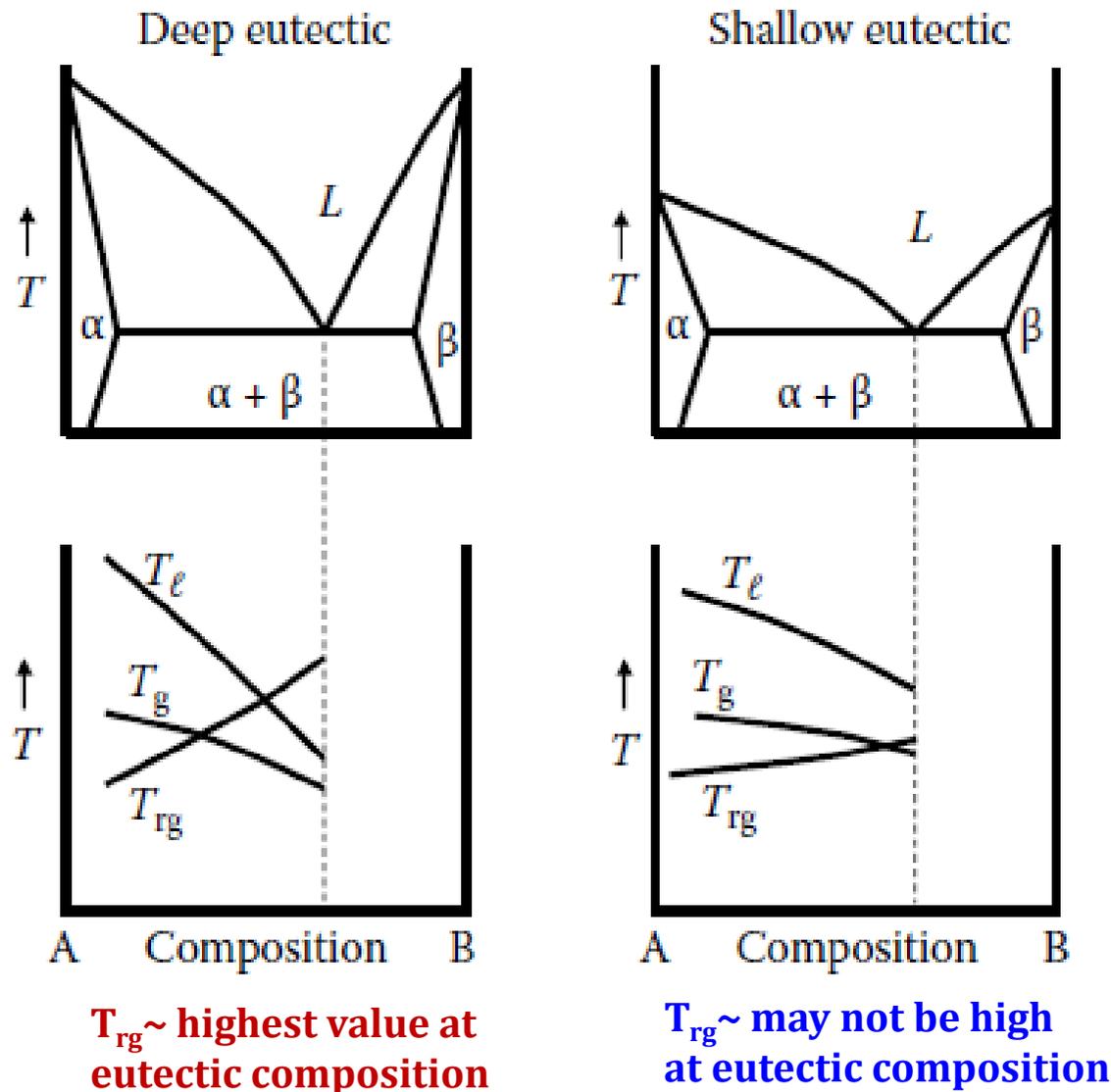
FIGURE 3.3

Schematic variation of the glass transition temperature, T_g, liquidus temperature, T_ℓ, the reduced glass transition temperature, T_{rg}, in two different types of eutectic systems—deep eutectic and shallow eutectic.

Ribbons of about 20–50 μm in thickness were produced by melt-spinning techniques in a number of binary alloy systems near eutectic compositions and they were confirmed to be glassy. Some of the most investigated eutectic compositions are found in Fe–B, Pd–Si, Cu–Zr, Ni–Nb, Ni–Ta, etc., alloy systems [1,2]. There have been some reports in recent years of "bulk" (?) metallic glass synthesis in binary alloy systems such as Ca–Al [59], Cu–Hf [49], Cu–Zr [51], Ni–Nb [37], and Pd–Si [42]. But, the maximum diameters of these binary alloy glassy rods were only 1 or 2 mm, and even then, some of these alloy glasses contained nanocrystalline particles embedded in the glassy matrix [60]. This point will be further discussed in detail in later chapters. But, the important point here is that the "bulk" glassy phase is produced not at the eutectic composition, but, at off-eutectic compositions. Further, the highest GFA, i.e., the composition at which glass formation was the easiest or the maximum diameter of the BMG rod could be obtained, was located away from the eutectic composition. The best glass-forming compositions have been reported to be at 35 at.% Hf in Cu–Hf, 36 at.% Zr in Cu–Zr, 38 at.% Nb in Ni–Nb, and 19 at.% Si in Pd–Si alloy systems. But, the eutectic compositions in these alloy systems are at 33.0 and 38.6 at.% Hf in Cu–Hf, 38.2 at.% Zr in Cu–Zr, 40.5 at.% Nb in Ni–Nb, and 17.2 at.% Si in Pd–Si systems [61]. Similarly, it was reported that while a nearly fully glassy rod with 12 mm diameter could be obtained at an off-eutectic composition near $La_{62}Al_{15.7}(Cu,Ni)_{22.3}$, only a 1.5 mm diameter rod could be obtained in a fully glassy condition for the eutectic alloy of $La_{66}Al_{14}(Cu,Ni)_{20}$ [52].
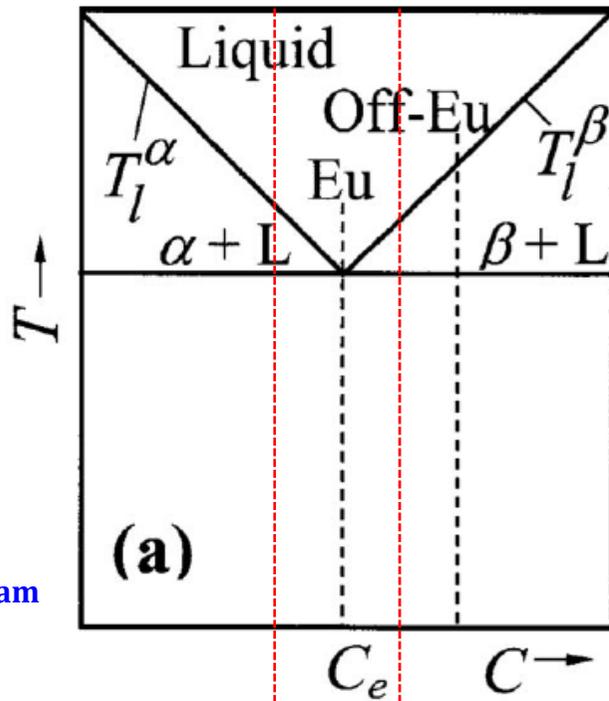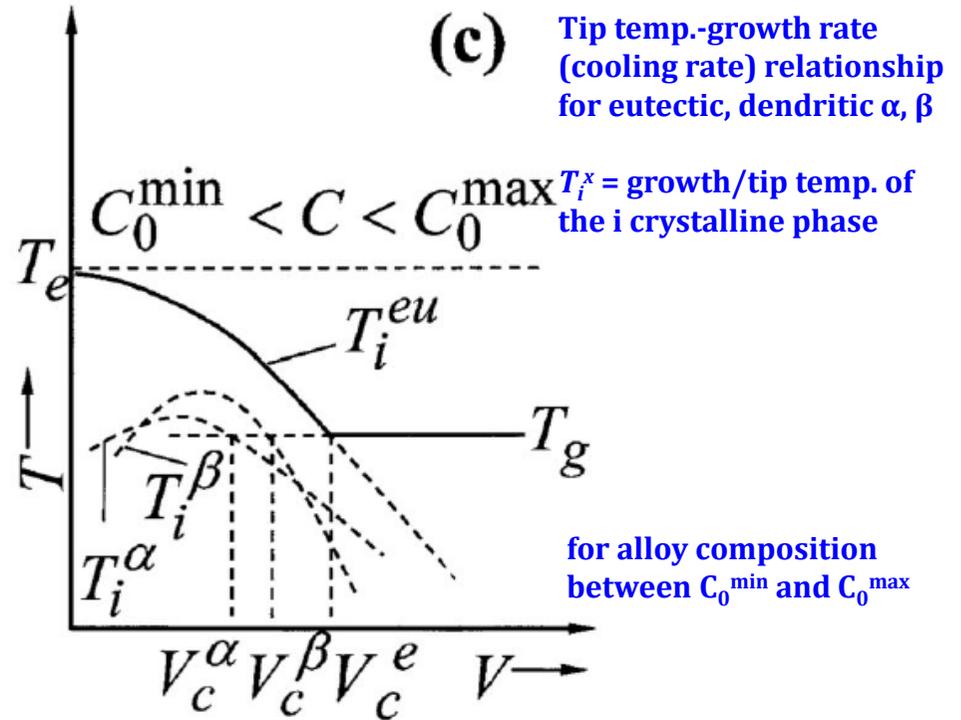
**(a)** Part of a regular Eutectic phase diagram

Liquid

Off-Eu

Eu

T_l^α $\alpha + L$ $\beta + L$ T_l^β

$T \rightarrow$

C_e $C \rightarrow$

(b) Glass-forming and Composite-forming Zones (symmetrical about eutectic composition)

Omitting the Negligible G effects at high V, a glass-forming zone: growth rate range over which a given alloy with composition C becomes a glass.

Glass

$\alpha +$ Glass $\beta +$ Glass

V_c^e

$\alpha +$ Eu $\beta +$ Eu

Eu

$V \rightarrow$

C_0^{min} C_e C_0^{max} $C \rightarrow$

(c) Tip temp.-growth rate (cooling rate) relationship for eutectic, dendritic α, β

T_i^x = growth/tip temp. of the i crystalline phase

$C_0^{min} < C < C_0^{max}$

T_e T_i^{eu}

T_i^β T_g

T_i^α

for alloy composition between C_0^{min} and C_0^{max}

$T \rightarrow$

V_c^α V_c^β V_c^e $V \rightarrow$

(d) $C > C_0^{max}$

T_l^β

T_e T_i^{eu} T_i^β

T_i^α T_g

for alloy composition of $C > C_0^{max}$

$T \rightarrow$

V_c^α V_c^e V_c^β $V \rightarrow$
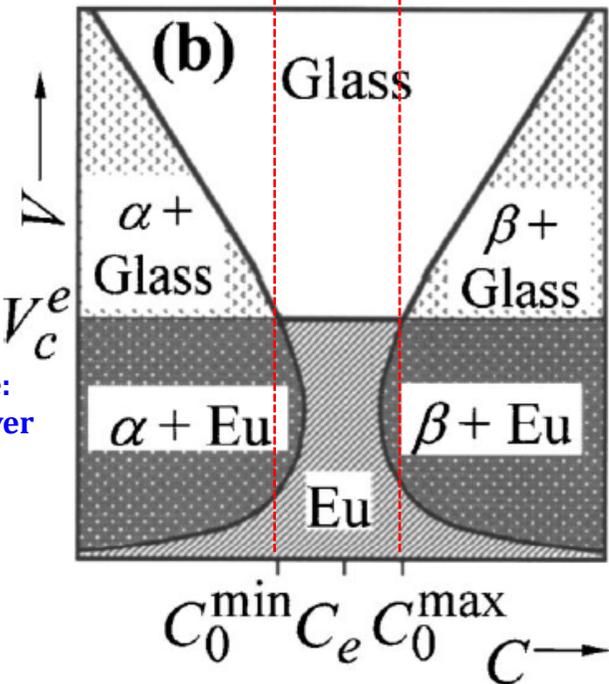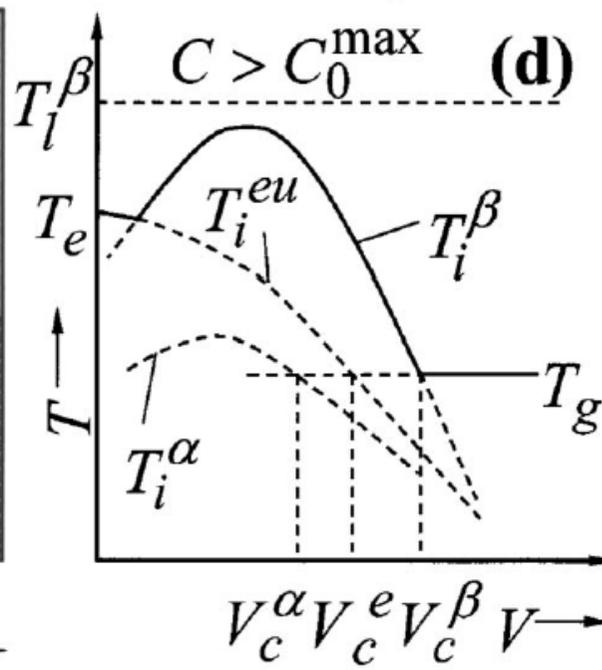
1. Growth 억제를 통한 비정질 형성 조건

▶ Glass가 생성될 조건

    ↳ Crystal nucleation이 일어나지 않을 때

    ↳ Growth of the nuclei가 억제될 때

➡ "T_g > growth temperature of any of the possible crystalline phases"

▶ Growth/Tip temperature of i phase, T_i^x

= Thermodynamic equilibrium temp. − undercooling required for growth

▶ Upon cooling, the phase having the highest T_i^x is kinetically the most stable one.

➡ $$T_g \geq T_i^x (x = eu, \alpha, \beta, ...)$$

$$T_g \geq T_i^{eu}, \quad T_g \geq T_i^{\alpha}, \quad \text{and } T_g \geq T_i^{\beta}$$
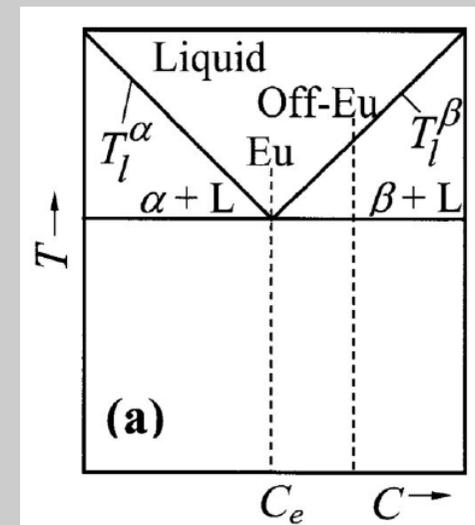
    : "Glass former의 조건"

▶ T_i^x : V(growth rate) 의 함수 ▶ glass가 형성될 조건

$$T_i^{eu} = T_e - K_e V^{1/2},$$

$$T_i^{\alpha} = T_l^{\alpha} - \frac{GD}{V} - K_{\alpha} V^n,$$

$$T_i^{\beta} = T_l^{\beta} - \frac{GD}{V} - K_{\beta} V^n,$$

$$V \geqslant V_c^e \text{ when } C_0^{\min} \leqslant C \leqslant C_0^{\max}, \quad T_i^{eu} = T_g, V = V_c^e$$

$$V \geqslant V_c^{\alpha} \text{ when } C < C_0^{\min}, \quad T_i^{\alpha} = T_g, V = V_c^{\alpha}$$

$$V \geqslant V_c^{\beta} \text{ when } C > C_0^{\max}, \quad T_i^{\beta} = T_g, V = V_c^{\beta}$$
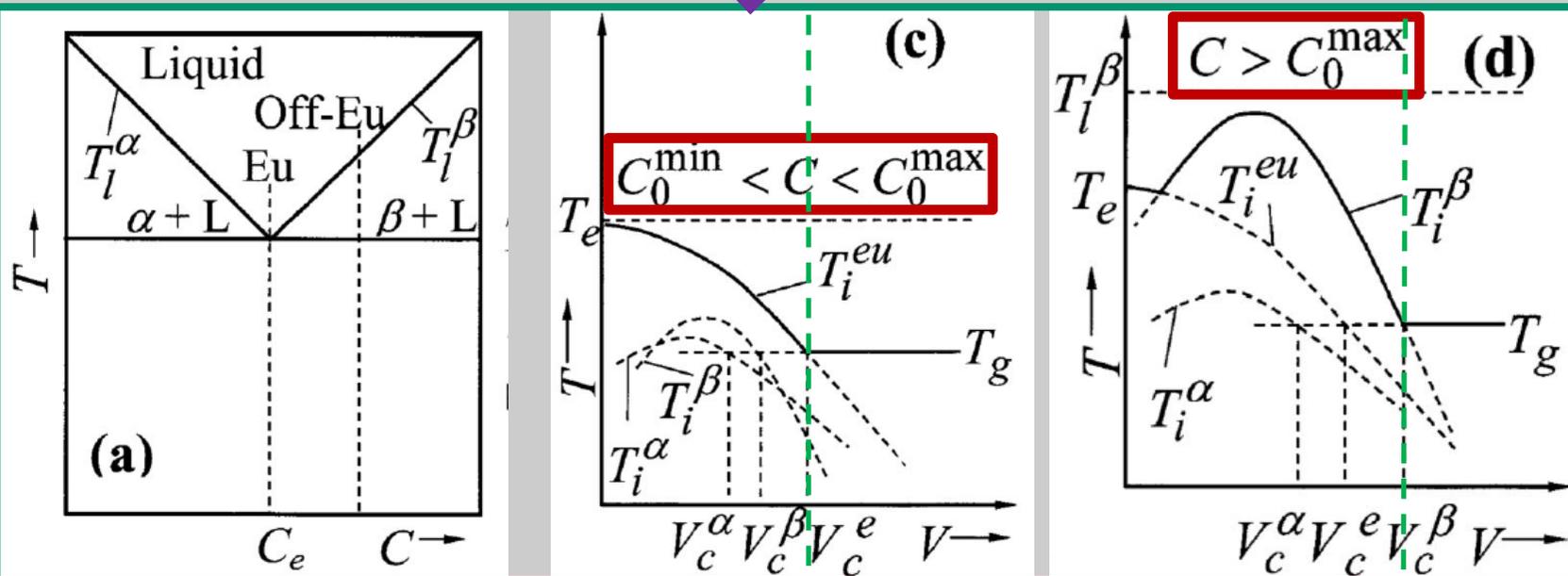
$$V_c^e = \frac{(T_e - T_g)^2}{K_e^2}, \quad \text{**independent to composition**}$$

$$V_c^\alpha = \frac{[m_\alpha(C - C_e) + T_e - T_g]^{1/n}}{K_\alpha^{1/n}},$$

$$V_c^\beta = \frac{[m_\beta(C - C_e) + T_e - T_g]^{1/n}}{K_\beta^{1/n}},$$
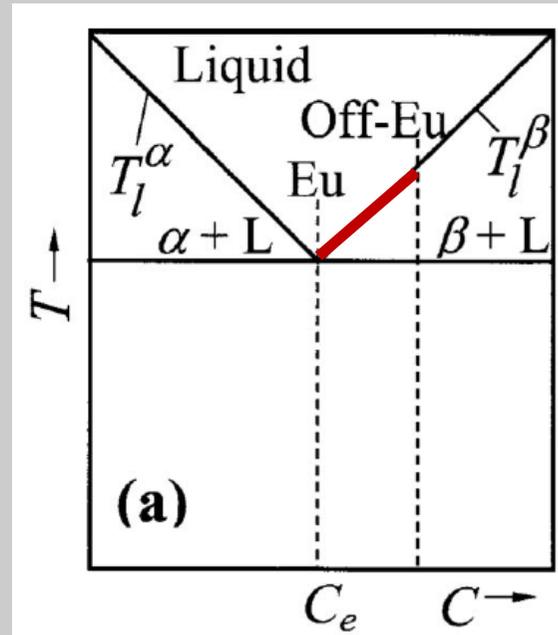

$$\frac{T_l^\alpha - T_e}{C - C_e} = m_\alpha$$

$$\frac{T_l^\beta - T_e}{C - C_e} = m_\beta$$
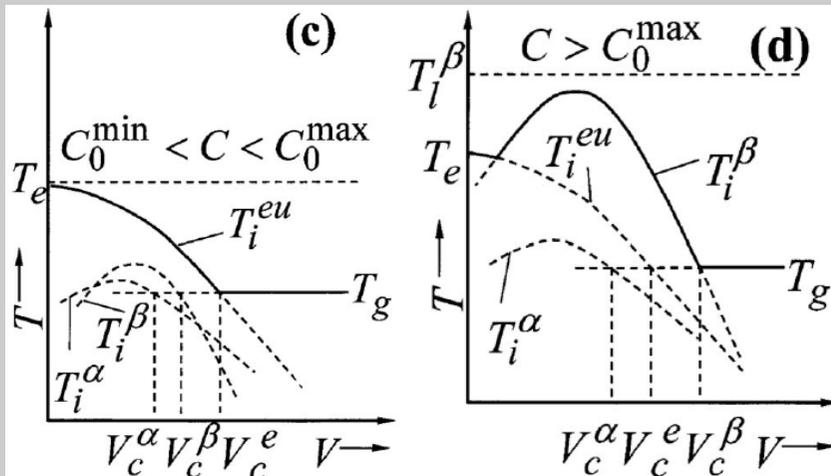
- V_c^e 가 maximum이 되는 $C_0^{min} \leq C \leq C_0^{max}$ 에서 가장 좋은 GFA를 가짐
- T_e 와 T_g 의 차이가 작을수록 GFA가 좋음
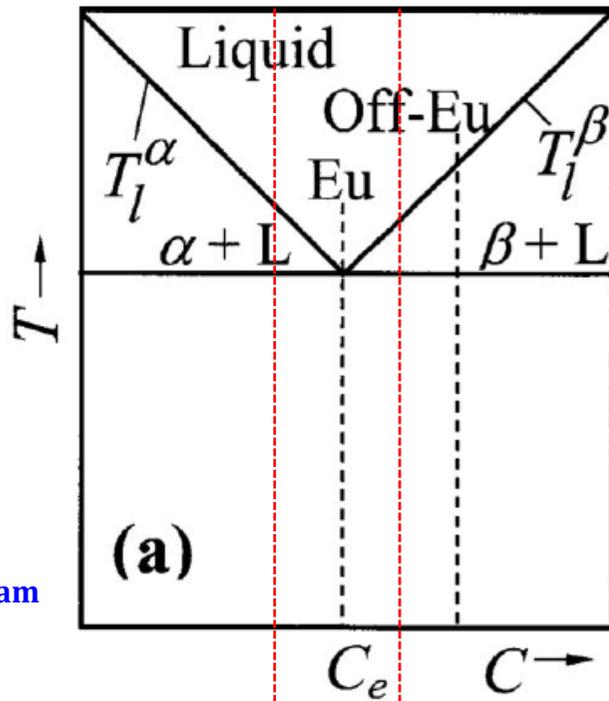
Part of a regular Eutectic phase diagram
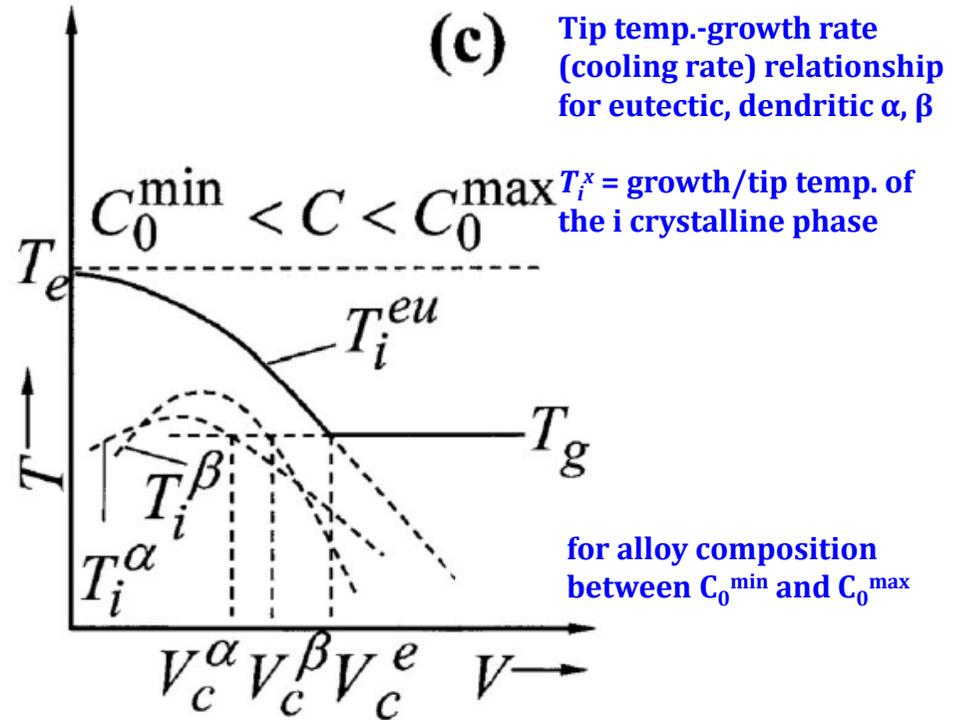
(a)

Liquid

Off-Eu

Eu

T_l^α T_l^β

$\alpha + L$ $\beta + L$

$T \rightarrow$

C_e $C \rightarrow$

**Glass-forming and Composite-forming Zones (symmetrical about eutectic composition)**

Omitting the Negligible G effects at high V, a glass-forming zone: growth rate range over which a given alloy with composition C becomes a glass.

**(b)**

Glass

$\alpha +$ Glass $\beta +$ Glass

V_c^e

$\alpha +$ Eu $\beta +$ Eu

Eu

$V \rightarrow$

C_0^{min} C_e C_0^{max}

$C \rightarrow$

(c)

Tip temp.-growth rate (cooling rate) relationship for eutectic, dendritic α, β

$C_0^{min} < C < C_0^{max}$

T_i^x = growth/tip temp. of the i crystalline phase

T_e

T_i^{eu}

T_g

T_i^β

T_i^α

$T \uparrow$

for alloy composition between C_0^{min} and C_0^{max}

V_c^α V_c^β V_c^e $V \rightarrow$

(d)

$C > C_0^{max}$

T_l^β

T_e

T_i^{eu} T_i^β

T_i^α

T_g

$T \uparrow$

for alloy composition of $C > C_0^{max}$

V_c^α V_c^e V_c^β $V \rightarrow$

C_e 가

$$C_0^{min} \leq C \leq C_0^{max}$$
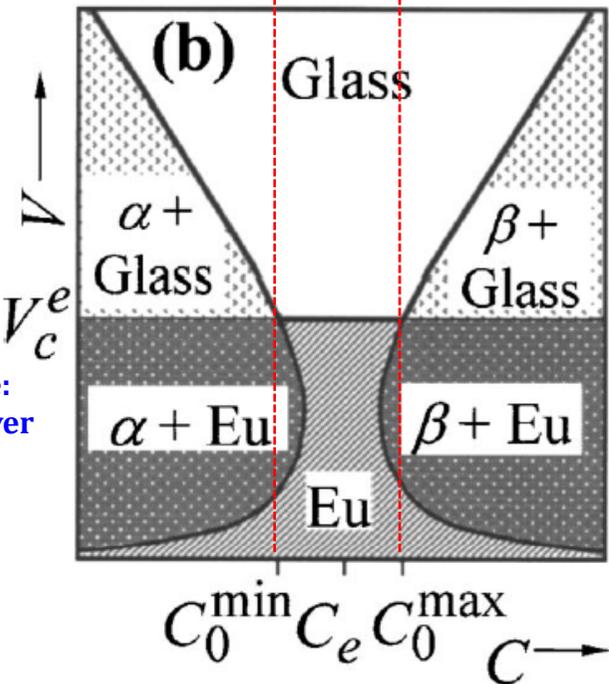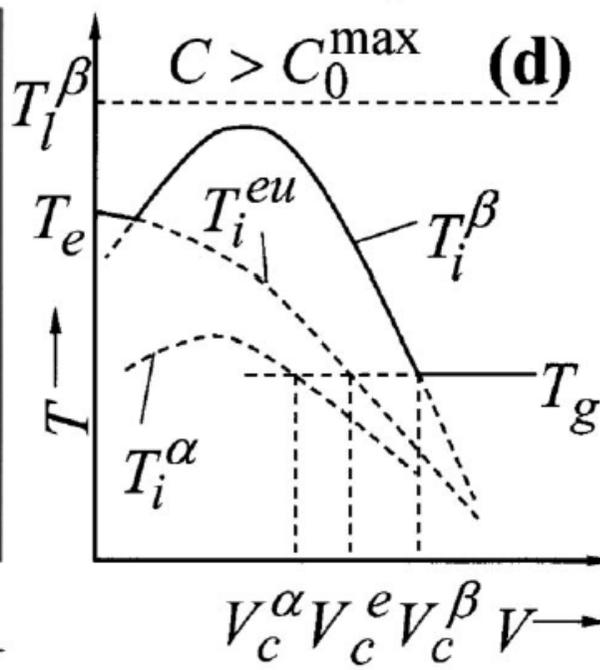
외부에 있음
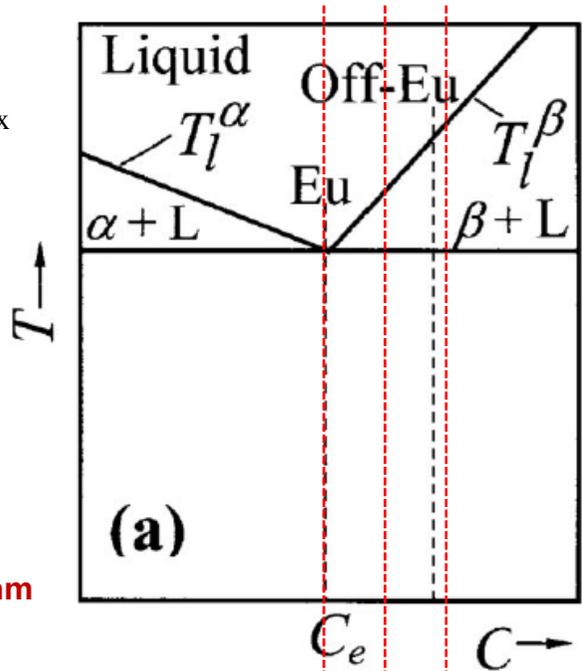
Part of a irregular eutectic phase diagram
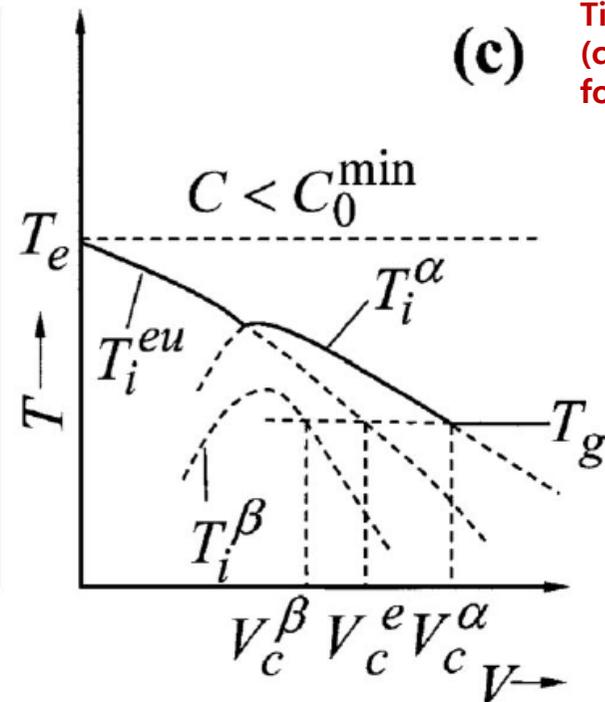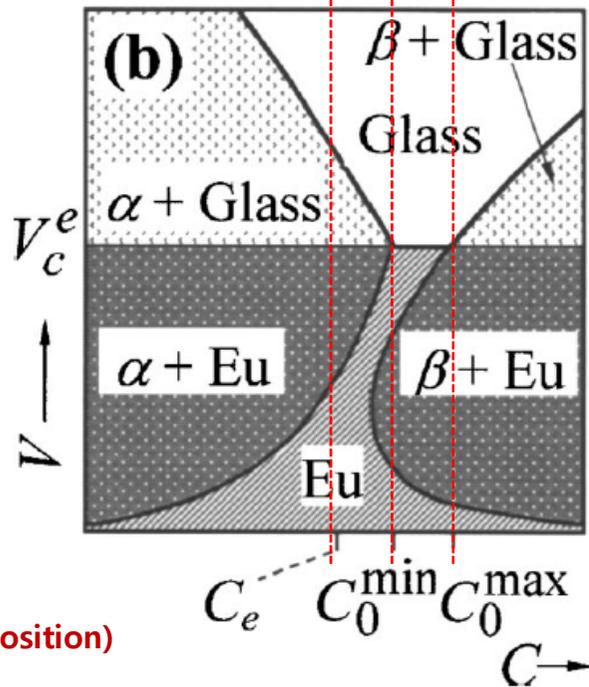
Glass-forming and Composite-forming Zones (asymmetrical about eutectic composition)

Tip temp.-growth rate (cooling rate) relationship for eutectic, dendritic α, β

for alloy composition of C < C_0^{min}

for alloy composition between C_0^{min}< C <C_0^{max}

(a) Liquid, Off-Eu, T_l^α, T_l^β, Eu, $\alpha + L$, $\beta + L$, C_e, T, C

(b) β + Glass, Glass, α + Glass, $\alpha + Eu$, $\beta + Eu$, Eu, V_c^e, V, C_e, C_0^{min}, C_0^{max}, C

(c) $C < C_0^{min}$, T_e, T_i^{eu}, T_i^α, T_g, T_i^β, V_c^β, V_c^e, V_c^α, V, T

(d) $C_0^{min} < C < C_0^{max}$, T_l^β, T_e, T_i^{eu}, T_i^β, T_g, T_i^α, V_c^α, V_c^β, V_c^e, V, T
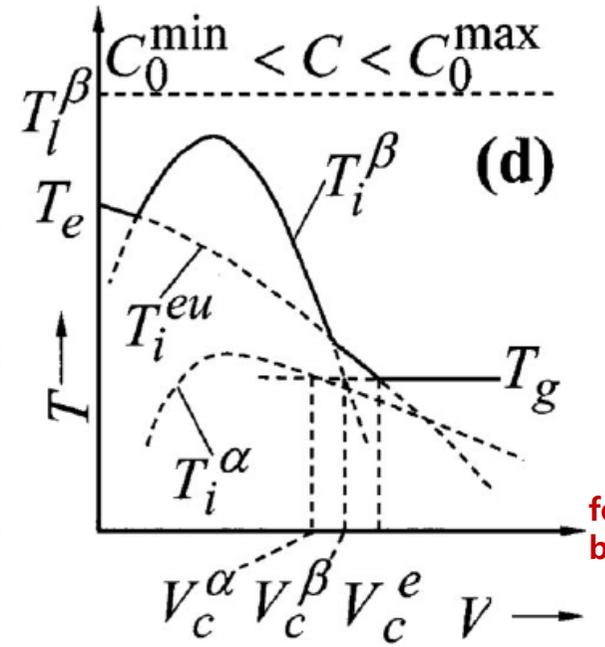
Schematic diagram showing skewed eutectic coupled zone and its relation to the glass-forming ability

(a)

T

Eutectic

Off-Eu

α

Eu

Eu+β

Eu+α

β

A C_0 ⟶   B

A eutectic system with skewed coupled zone

(c)

T

Eutectic alloy

T_E

eutectic

α

β

T_g

$\dot{T}_1(V_1)$ $\dot{T}_c(V_c)$ $\dot{T}_a(V_a)$ $\dot{T}(V)$

Growth temp. of the constituents as a function of cooling rate (growth rate) for the eutectic alloy

(b)

T

Eutectic

Off-Eu

α

Eu

Eu+α

Eu+β

Glass+β

β

Glass+α

Glass

A C_0 ⟶   B
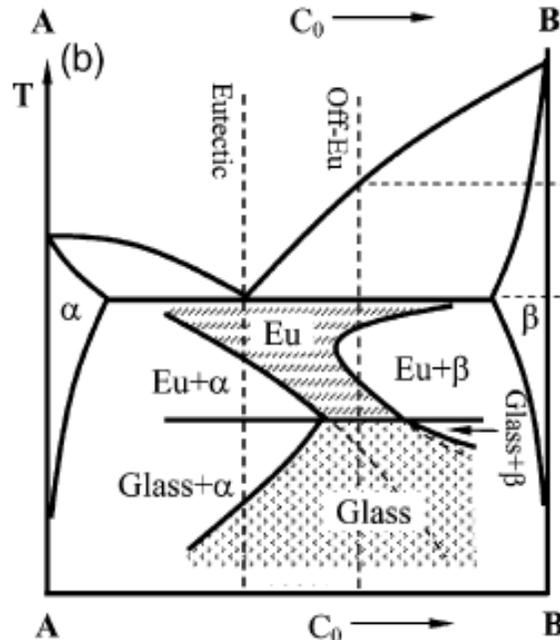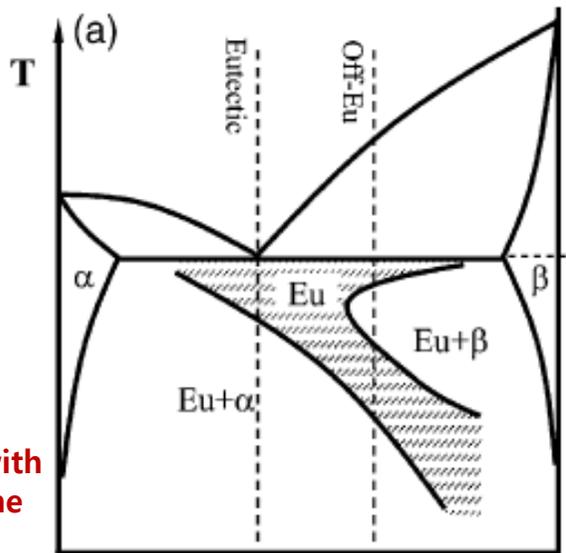
Glass forming and composite forming regions related to the skewed coupled zone

(d)

T

Off-eutectic alloy

T_L

T_E

eutectic

β

T_g

α

$\dot{T}_a(V_a)$ $\dot{T}(V)$
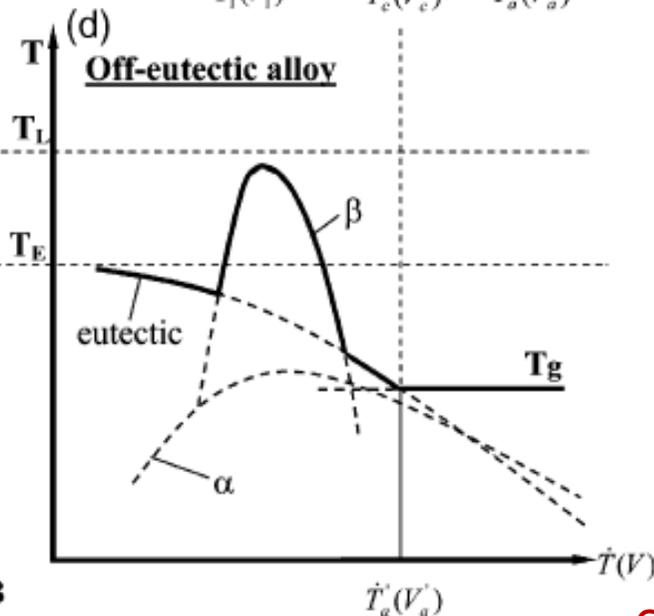
Growth temp. of the constituents as a function of CR (GR) for an off-eutectic alloy

Composites & Glass forming composition

< 대칭 공정 합금 >
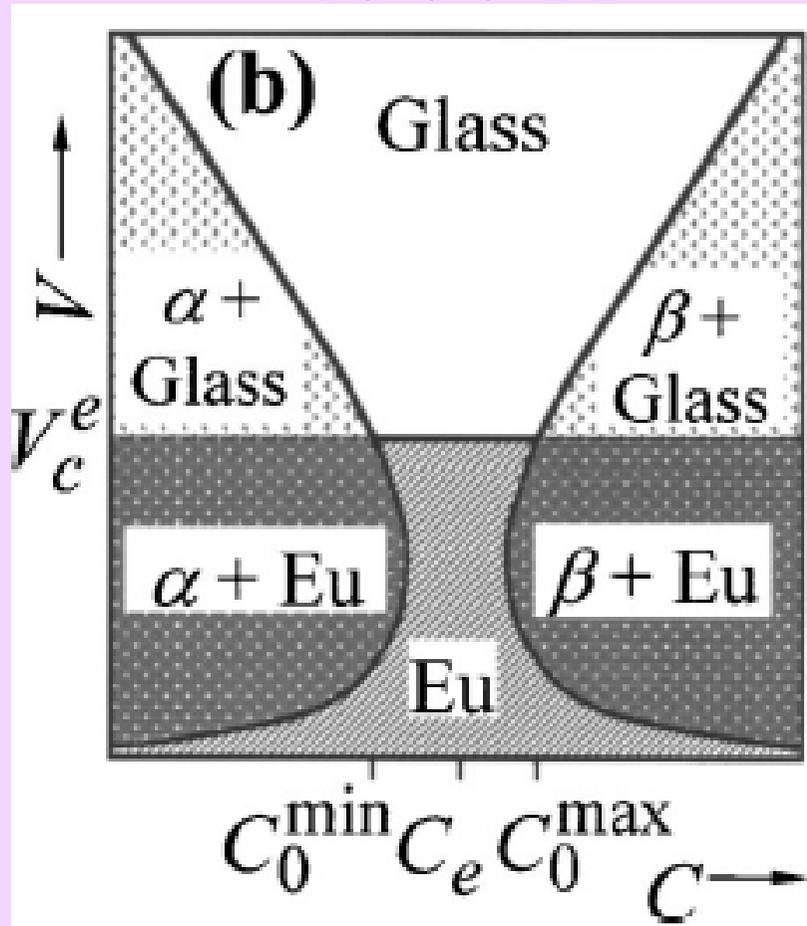
< 비대칭 공정 합금 >
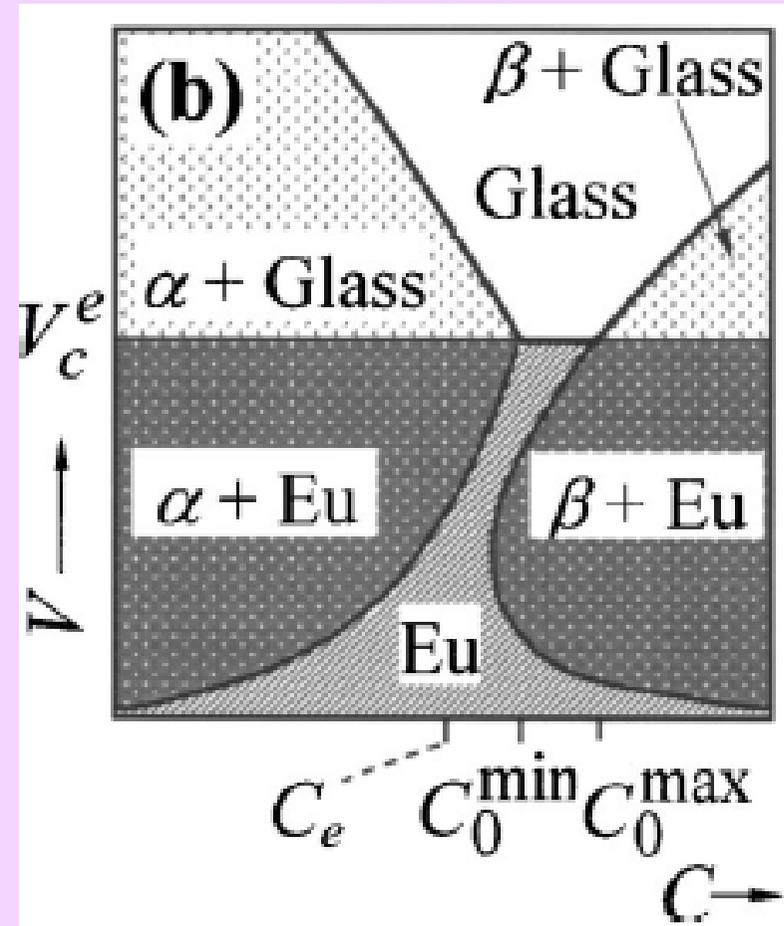
▶ **Glass region은 서로 다른 제2상을 가진 composite으로 둘러싸여 있음**

⟹ **Maximum GFA를 갖는 조성을 찾을 때 사용**

Composites & Glass forming composition
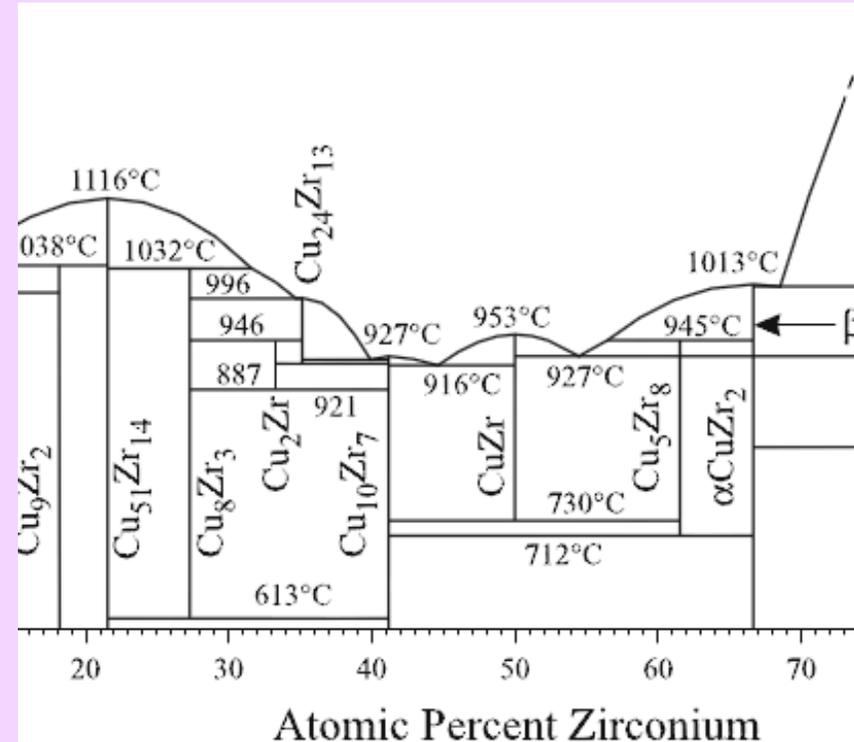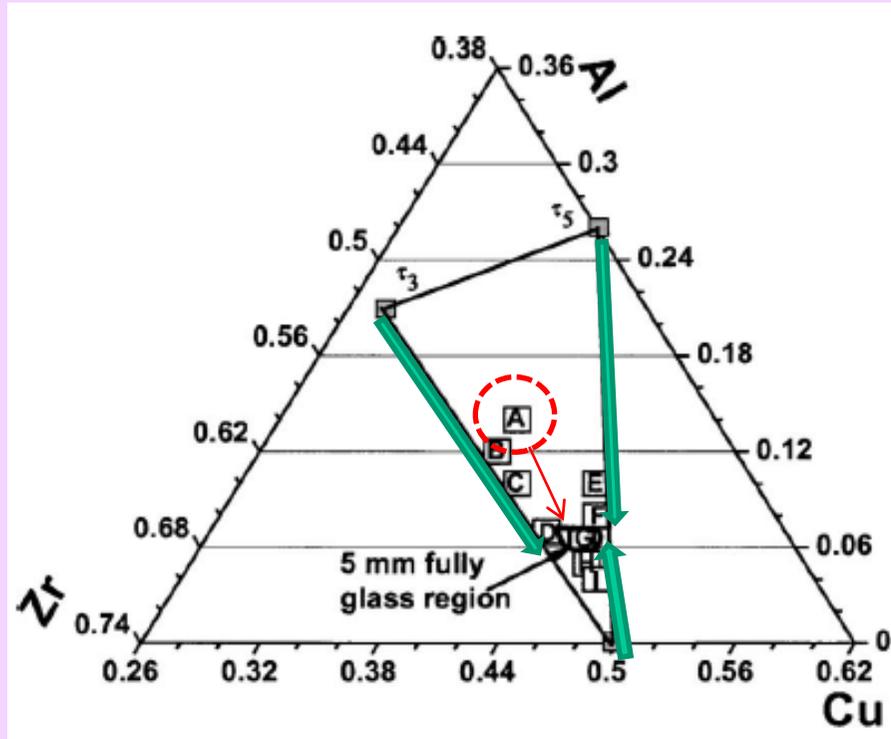

▶ 각 line에서 ZrCu, τ_3 , τ_5 의 ternary eutectic reaction 근방에 있을 것으로 예상

1. A($Zr_{48}Cu_{38}Al_{14}$) : eutectic 조성이지만 glass 혹은 composite조차 생기지 않음

   ⇒ Cu-Zr 합금에서 Liquidus line의 기울기가 큰 Zr쪽으로 이동

Composites & Glass forming composition
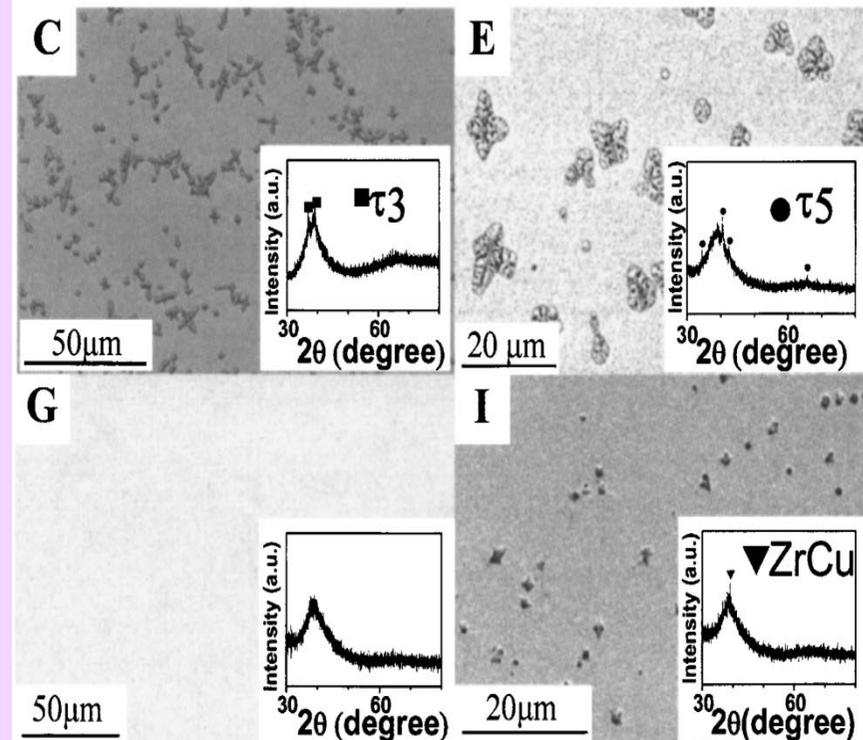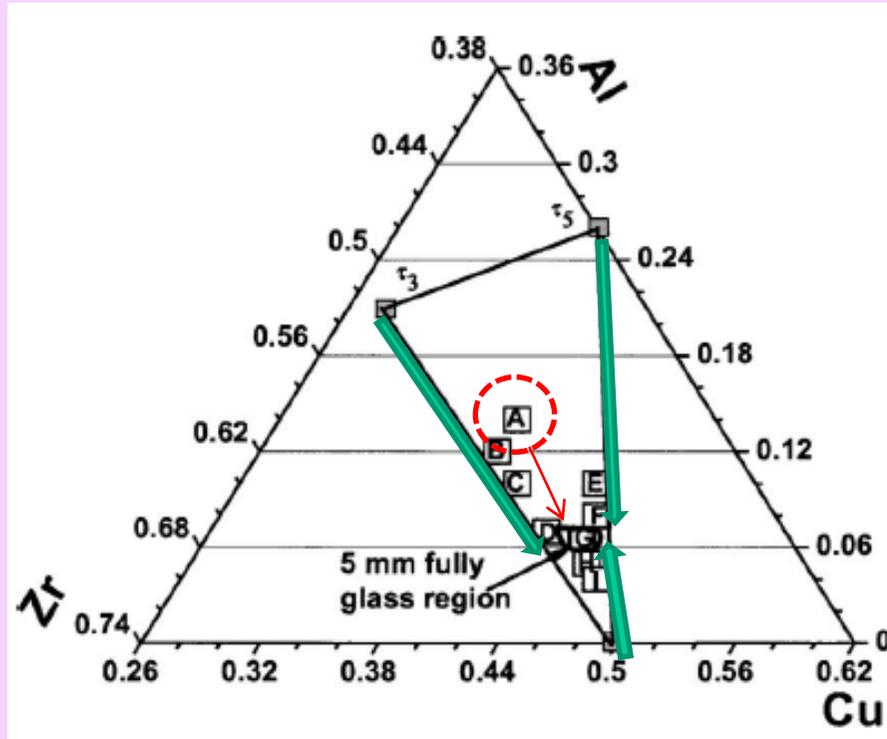
2. 화살표를 따라 τ_3+glass (**B,C,D**), τ_5 + glass (**E,F**), ZrCu + glass (**I,H**)가 나오는 composite forming region을 구함(casted into 5 mm-diam copper mold)

➡ **G** 점을 기준으로 제 **2** 상이 변함

➡ **G** 에서 **full glass**가 생김

3.5 Topological Model (Structural aspect for glass formation)

Metallic glasses produced by RSP methods in the form of thin ribbons have been traditionally classified into two groups, viz., metal–metalloid and metal–metal types. Structural models of the metal-metalloid-type metallic glasses have identified that the best composition to form a glass is one that contains about 80 at.% of the metal component and 20 at.% of the metalloid component. The actual glass composition ranges observed are 75–85 at.% of the metal and 15–25 at.% of the metalloid. As stated in Chapter 2, the 80 at.% of the metal can be either a single transition metal or a combination of transition metals or one or a combination of noble metals. Similarly, the 20 at.% of the metalloid content could be made up of just one component or a mixture of a number of components. In the case of metal-metal types, however, there is no such restriction on compositions. Metal-metal-type metallic glasses have been observed to form over a wide range of compositions, starting from as low as 9 at.% of solute. Some typical compositions in which metal-metal type glasses have been obtained are $Cu_{25-72.5}Zr_{27.5-75}$, $Fe_{89-91}Zr_{9-11}$, $Mg_{68-75}Zn_{25-32}$, $Nb_{55}Ir_{45}$, and $Ni_{58-67}Zr_{33-42}$ [65].

* Metallic glass : Randomly dense packed structure

1) Atomic size difference: TM – metalloid (M, ex) Boron)

→ **M is located at interior of the tetrahedron of four metal atoms (TM$_4$M)**

→ **denser** ⟹ **by increasing resistivity of crystallization, GFA ⬆**

→ **Ex) Fe-B: tetrahedron with B on the center position**

       1) interstitial site, B= simple atomic topology

       2) skeleton structure

       3) bonding nature: close to covalent bonding

Irrespective of the actual size of the voids and whether the above model is valid or not, it is of interest to note that the metal-metalloid-type binary phase diagrams exhibit deep eutectics at around a composition of 15–25 at.% metalloid. Some typical examples are Fe–B (17 at.% B), Au–Si (18.6 at.% Si), and Pd–Si (17.2 at.% Si). Therefore, the concepts of deep eutectics and structural models also seem to converge in obtaining glasses in the (transition or noble) metal-metalloid types.

3.5.2. Egami and Waseda Criterion

One of the possible ways by which a crystalline metallic material can become glassy is by the introduction of lattice strain. The lattice strain introduced disturbs the crystal lattice and once a critical strain is exceeded, the crystal becomes destabilized and becomes glassy. In fact, Egami takes pains to state that "In general, alloying makes glass formation easier, not because alloying stabilizes a glass, but because it destabilizes a crystal" [72, p. 576]. Using the atomic scale elasticity theory, Egami and Waseda [73] calculated the atomic level stresses in the solid solution (the solute atoms are assumed to occupy the substitutional lattice sites in the solid solution) and the glassy phase. They observed that in a glass, neither the local stress fluctuations nor the total strain energy vary much with solute concentration, when normalized with respect to the elastic moduli. But, in a solid solution, the strain energy was observed to increase continuously and linearly with solute content. Thus, beyond a critical solute concentration, the glassy alloy becomes energetically more favorable than the corresponding crystalline lattice. From the vast literature available on the formation of binary metallic glasses obtained by RSP methods, the authors noted that a minimum solute concentration was necessary in a binary alloy system to obtain the stable glassy phase by RSP methods.

2) min. solute content, C_B^*: empirical rule By Egami & Waseda: in A-B binary system

$$C_B^{min} \left| \frac{(v_B - v_A)}{v_A} \right| = C_B^{min} \left| \left(\frac{r_B}{r_A}\right)^3 - 1 \right| \approx 0.1$$

v: atomic volume
A: matrix, B: solute

minimum concentration of B for glass formation 존재

→ **Inversely proportional to atomic volume mismatch**
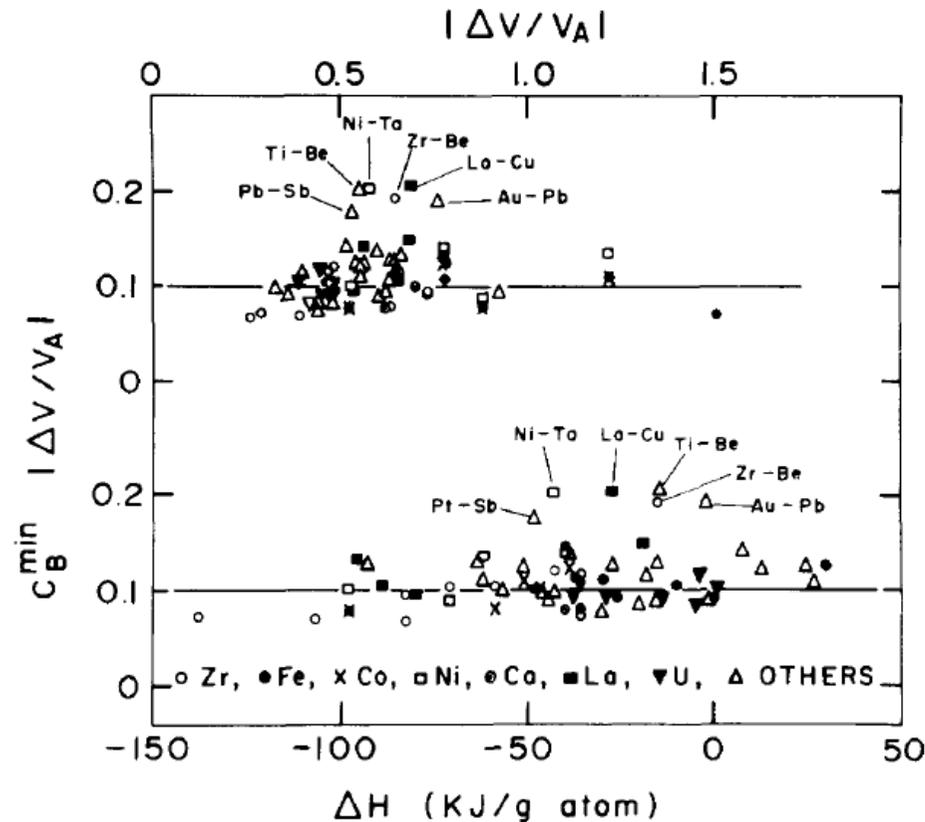
Fig. 1. Relation between $|\lambda_0| = C_B^{min} |\Delta v/v_A|$, and $|\Delta v/v_A|$ and ΔH, for 66 binary systems which can be vitrified by liquid quenching.

3.5.3. Nagel and Tauc Criterion

Nagel and Tauc [74,75] proposed that a glass is most likely to form if its electronic energy lies in a local metastable minimum with respect to composition change. They showed that if the structure factor corresponding to the first strong peak of the diffuse scattering curve, K_p, satisfies the relationship $K_p = 2 k_F$, where k_F is the wave vector at the Fermi energy, then the electronic energy does indeed occupy a local minimum.

Fig. 7. Schematic structure factor a(K)

Fig. 11. a(K) versus K for lower and higher temperatures
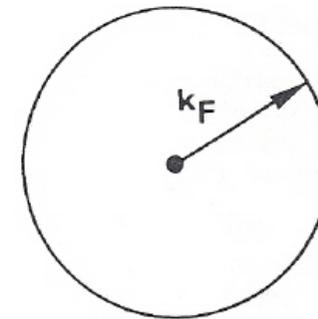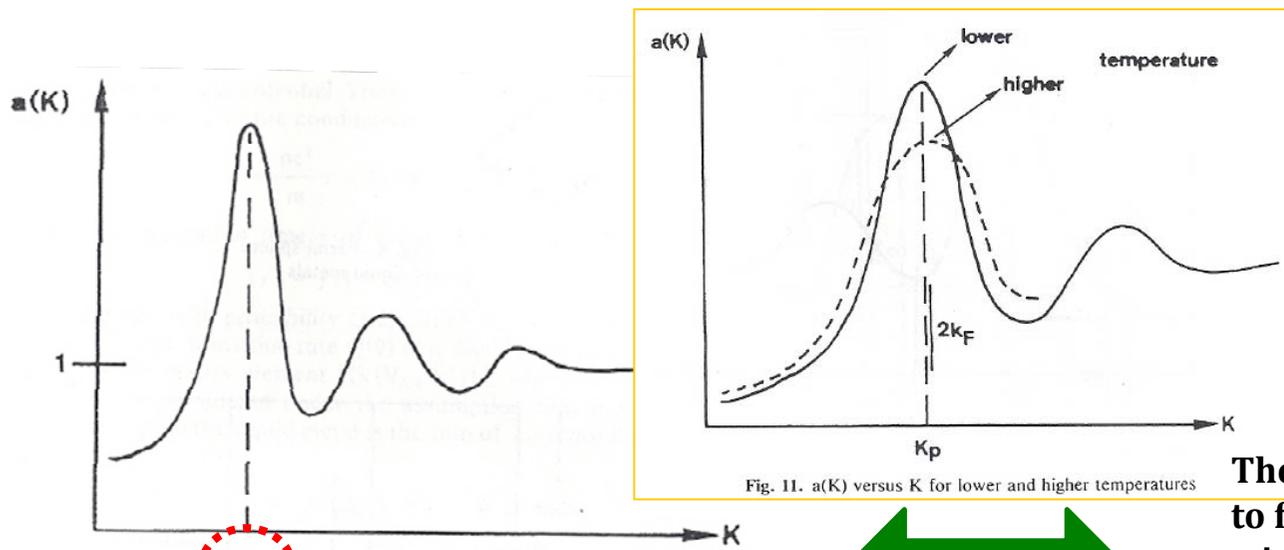
$$Kp = 2 \ k_F$$

The conduction electrons are suppose to form a degenerate free-electron gas with a spherical **Fermi surface**.

$$2K_F = 2(3\pi^2 n)^{1/3} = 2\left(\frac{3\pi^2}{eR_H}\right)^{1/3}$$

a(K) Fourier transform of the pair correlation function g(r)

Kp Nearest neighbor distance of the liquid metal in K-space

: Diameter of Fermi surface